Article

Cell Reports

Quantitative Proteomics Identifies Serum Response Factor Binding Protein 1 as a Host Factor for Hepatitis C Virus Entry

Graphical Abstract

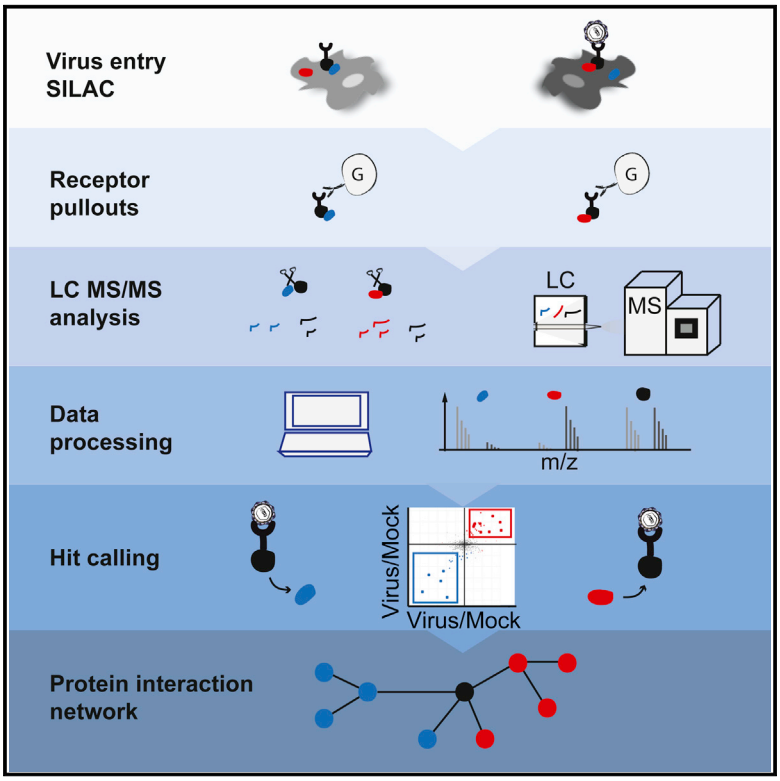

Highlights

- Hepatitis C virus binding alters host protein interactions with the receptor CD81
- Six out of 26 virus-dependent CD81-interacting proteins promote virus entry
- SRFBP1 binds CD81 and aids infection of all HCV, but not VSV, genotypes
- SRFBP1 is membrane-associated and required for HCV entry

Authors

Gisa Gerold, Felix Meissner, Janina Bruening, ..., Matthias Mann, Charles M. Rice, Thomas Pietschmann

Correspondence

gisa.gerold@twincore.de (G.G.), thomas.pietschmann@twincore.de (T.P.)

In Brief

Hepatitis C virus (HCV) enters human hepatocytes through a multistep mechanism. Gerold et al. apply quantitative proteomics to define the protein network responsible for HCV entry and identify SRFBP1 as a partner for the virus receptor CD81.

Gerold et al., 2015, Cell Reports *12*, 864–878
August 4, 2015
http://dx.doi.org/10.1016/j.celrep.2015.06.063

CellPress

OPEN ACCESS
CellPress

Cell Reports
Article

Quantitative Proteomics Identifies Serum Response Factor Binding Protein 1 as a Host Factor for Hepatitis C Virus Entry

Gisa Gerold,[1,2,*] Felix Meissner,[3] Janina Bruening,[1] Kathrin Welsch,[1] Paula M. Perin,[1] Thomas F. Baumert,[4] Florian W. Vondran,[5] Lars Kaderali,[6] Joseph Marcotrigiano,[7] Abdul G. Khan,[7] Matthias Mann,[3] Charles M. Rice,[2] and Thomas Pietschmann[1,*]

[1]Insitute for Experimental Virology, TWINCORE, Centre for Experimental and Clinical Infection Research, a joint venture between the Medical School Hannover and the Helmholtz Centre for Infection Research, 30165 Hannover, Germany
[2]Center for the Study of Hepatitis C, Laboratory of Virology and Infectious Disease, the Rockefeller University, New York, NY 10065, USA
[3]Department of Proteomics and Signal Transduction, Max Planck Institute for Biochemistry, 82152 Martinsried, Germany
[4]Inserm Unit 1110, Université de Strasbourg, Strasbourg 67000, France
[5]Department of General, Visceral and Transplant Surgery, Hannover Medical School, 30165 Hannover, Germany
[6]Institute for Medical Informatics and Biometry (IMB), Medical School, University of Technology Dresden, 01307 Dresden, Germany
[7]Center for Advanced Biotechnology and Medicine, Department of Chemistry and Chemical Biology, Rutgers University, Piscataway, NJ 08854, USA
*Correspondence: gisa.gerold@twincore.de (G.G.), thomas.pietschmann@twincore.de (T.P.)
http://dx.doi.org/10.1016/j.celrep.2015.06.063

SUMMARY

Hepatitis C virus (HCV) enters human hepatocytes through a multistep mechanism involving, among other host proteins, the virus receptor CD81. How CD81 governs HCV entry is poorly characterized, and CD81 protein interactions after virus binding remain elusive. We have developed a quantitative proteomics protocol to identify HCV-triggered CD81 interactions and found 26 dynamic binding partners. At least six of these proteins promote HCV infection, as indicated by RNAi. We further characterized serum response factor binding protein 1 (SRFBP1), which is recruited to CD81 during HCV uptake and supports HCV infection in hepatoma cells and primary human hepatocytes. SRFBP1 facilitates host cell penetration by all seven HCV genotypes, but not of vesicular stomatitis virus and human coronavirus. Thus, SRFBP1 is an HCV-specific, pan-genotypic host entry factor. These results demonstrate the use of quantitative proteomics to elucidate pathogen entry and underscore the importance of host protein-protein interactions during HCV invasion.

INTRODUCTION

Virus entry describes the process of delivering viral genomes in a replication-competent manner into a naive host cell. Successful penetration of cells involves receptor binding, virion uptake, membrane fusion or perturbation, transport of nucleocapsids to replication competent cellular compartments, and uncoating (Yamauchi and Helenius, 2013). Virus receptors are more than attachment factors, functionally supporting cell entry by several means: they mediate formation of receptor platforms, induce conformational changes in virus surface molecules, transmit signals within the cell, and induce virus translocation along the membrane and into the cell (Mercer et al., 2010). A number of virus receptors, however, lack signaling domains. Consequently, these receptors must initiate the virus uptake program through ligand-dependent interaction with additional host proteins.

In this study, we focus on the entry mechanism of hepatitis C virus (HCV), an enveloped RNA virus infecting 160 million individuals worldwide (Gravitz, 2011; Lavanchy, 2011). Hepatitis C is a slowly progressing disease, which can cause liver fibrosis, cirrhosis, and hepatocellular carcinoma 15–25 years after contraction (Seeff, 2002). To date, hepatitis C is the number one indication for liver transplantation in North America and Europe. Unfortunately, re-infection of the graft liver by virus residing in peripheral reservoirs is almost universal and leads to accelerated disease progression. For post-transplant patients, interfering with the entry of HCV into the engrafted hepatocytes would be a promising preventive treatment.

HCV penetration is a multistep process requiring the four entry factors scavenger receptor class B member 1 (SR-BI), CD81, claudin-1 (CLDN1), and occludin (OCLN) (Evans et al., 2007; Pileri et al., 1998; Ploss et al., 2009; Scarselli et al., 2002). CD81 is a central player in HCV entry as it directly binds the HCV E2 surface glycoprotein, renders it fusion competent (Pileri et al., 1998; Rajesh et al., 2012; Sharma et al., 2011), and activates the HCV entry cofactor epidermal growth factor receptor (EGFR) (Diao et al., 2012; Gerold and Rice, 2011; Lupberger et al., 2011). Moreover, CD81 is thought to laterally translocate with the virions to tight junctions, where CLDN1 and OCLN reside (Brazzoli et al., 2008). Finally, CD81 and CLDN1 co-internalize with the virus into endosomes (Farquhar et al., 2012). How CD81 orchestrates HCV uptake remained elusive. As a scaffolding protein, CD81 lacks intracellular signaling domains but coordinates protein-protein interactions in membrane microdomains termed

tetraspanin webs (Charrin et al., 2003; Montpellier et al., 2011). We hypothesized that the binding of HCV to CD81 triggers protein interactions, which in turn coordinate HCV uptake.

Here, we determined changes in the protein interaction network coordinated by CD81 during uptake of HCV particles using quantitative proteomics (Meissner and Mann, 2014). We found 26 HCV-dependent CD81 interactions. Consistent with our hypothesis, a subset of the receptor-interacting proteins promoted HCV infectivity. In particular, we identified serum response factor binding protein 1 (SRFBP1) as an HCV host factor, which forms a complex with CD81 and coordinates host cell penetration. The method described here is applicable to various steps in the life cycle of viruses and other microbes. It holds the promise of revealing critical pathogen-induced changes in host protein-protein interactions, thus guiding development of anti-infective strategies.

RESULTS

Quantitative Proteomics Identifies Virus Entry-Dependent Receptor Interactions

Quantitative proteomics allows the hypothesis-free characterization of protein-protein interactions between cellular states. Here, we use stable isotope labeling by amino acids in cell culture (SILAC) and quantitative interaction proteomics (Ong et al., 2002) to study host protein interactions with the HCV receptor CD81 upon HCV exposure. To this end, HCV permissive human hepatoma cells Huh-7 were labeled with heavy arginine (($^{15}N_4{}^{13}C_6$) Arg-10) and lysine (($^{15}N_2{}^{13}C_6$) Lys-8), achieving 95% incorporation of heavy amino acids into cellular proteins (heavy) or left unlabeled (light). As HCV induces clathrin-mediated endocytosis 15 min after binding (Coller et al., 2009), we incubated heavy Huh-7 cells for 15 min with HCV (J6/JFH-1 clone 2; MOI: 10) and light cells with non-infectious cell culture supernatants (forward label). To exclude isotope-specific effects, we swapped labels of the two conditions, so that light cells were HCV exposed and heavy cells mock treated (reverse label). Next, we affinity enriched CD81 and its interacting proteins (Figure S1A), combined proteins from HCV and uninfected samples, and digested proteins to peptides. Liquid chromatography (LC) coupled to mass spectrometry (MS) then identified, quantified, and distinguished peptides derived from HCV and uninfected conditions by their characteristic mass offset (Figures 1A and S1B).

LC-MS analysis revealed a total of 778 host proteins in CD81 co-immunoprecipitations (co-IPs). This high number is typical for affinity enrichment MS because it includes proteins, which non-specifically bind to the IP resin (Table S1) (Keilhauer et al., 2015). Subsequent data processing eliminates these background binders as described below. CD81 was detected in all co-IPs with high intensities independent of the presence of bound HCV (Figure S1C). To identify HCV-regulated protein-protein interactions, we next calculated the ratios of heavy over light protein abundances in cells with or without bound HCV. Protein quantification was reproducible as demonstrated by a median correlation of the SILAC ratios of $r^2 = 0.70$ and 0.81 for forward and reverse label samples, respectively. Here, we focused on proteins, which differed between the two experimental conditions, thereby excluding background binders, which are equally abundant in HCV and mock samples. As hypothesized, we identified 55 protein interactors, which quantitatively differed between HCV and mock samples. Among these HCV-dependent transient interactors are proteins that associate with CD81 (Figure 1B, upper right quadrant) or dissociate from CD81 upon virus exposure (Figure 1B, lower left quadrant).

We stratified HCV-dependent interactors of CD81 based on statistical significance, interaction strength, and biological relevance. In particular, inclusion criteria were a minimum of 2.1-fold change in CD81 interaction strength upon HCV exposure, liver expression, and non-nuclear localization. Of note, we additionally excluded ribosomal proteins in this study, although they might have a potential role in virus uncoating. A total of 26 proteins fulfilled these inclusion criteria, half of which dissociated from and the other half associated with CD81 upon virus binding (labeled data points in Figures 1B and 1C and Table S2; IntAct: IM-24070). Proteins that were exclusively quantified in the presence of HCV were assigned an infinite ratio, because the strength of interaction could not be determined. Known steady-state interaction partners of CD81 were absent from this transient interactome. Instead, we identified huntingtin-interacting-protein-1-related protein (HIP1R), a previously reported HCV entry cofactor and a known component of clathrin-coated pits (Coller et al., 2009). Taken together, we confirmed our hypothesis that HCV binding to CD81 alters its protein interaction network and that some HCV entry cofactors are transient CD81 interactors.

Next, we investigated whether certain molecular functions and cellular compartments were enriched in our transient CD81 interactome. Most proteins were membrane associated (49%) or cytoskeletal components (31%), with one-third being plasma membrane associated (Figure 1D; Table S3). Molecular function analysis revealed a strong enrichment for proteins with binding function (44%), catalytic activity (27%), and structural molecule activity (15%; Figure 1E; Table S4). Taken together, our gene ontology (GO) enrichment analysis reflects the fact that the HCV-CD81 complex laterally translocates along the plasma membrane (Brazzoli et al., 2008; Coller et al., 2009) with a need for interaction with plasma membrane and cytoskeletal proteins.

To further reveal interconnected cellular structures and processes enriched in the HCV entry-dependent protein pool, we integrated a DAVID-based clustering analysis in a STRING-based protein interaction map (Figure 1F). Notably, we found a cluster of six cellular junction proteins not previously reported in HCV entry. These proteins, which include adherens junction, desmosomal, and cell envelope constituents, are interconnected by reported protein-protein interactions. Furthermore, we found cytoskeletal proteins (spectrins; myosin-9) and a clathrin-coated pit protein (HIP1R), which is in line with the reported clathrin-mediated endocytosis of HCV (Blanchard et al., 2006). Finally, we found clusters of calcium- and metal-binding proteins as well as nuclear proteins, with a secondary cytoplasmic localization. All identified proteins with extracellular or plasma membrane localization dissociated from CD81 upon HCV binding (Figure 1F, blue label), whereas proteins localizing to endosomes or intracellular compartments associated with CD81 (Figure 1F, red label). This confirms the notion that the HCV-CD81 complex needs to

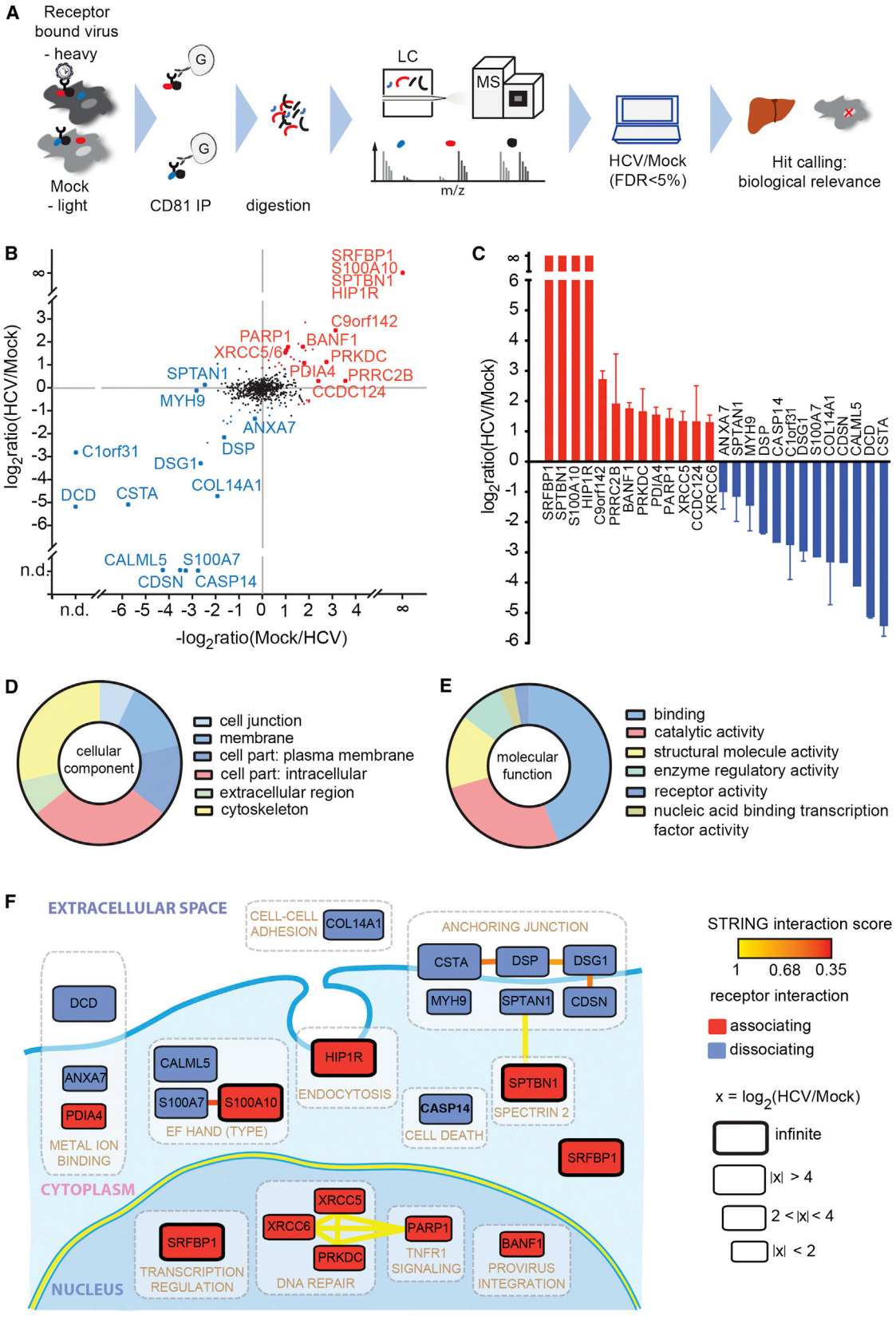

(legend on next page)

move out of plasma membrane microdomains to then get endocytosed. In summary, we identified 26 selected transient protein-receptor interactions during HCV entry including a known HCV entry cofactor and a cluster of junctional membrane proteins.

Virus-Dependent CD81-Binding Proteins Promote HCV Infectivity

We hypothesized that a subset of the 26 virus-dependent CD81-interacting proteins is required for productive virus entry. To test this, we silenced the 26 respective mRNAs and infected human hepatoma cells with a *Renilla* luciferase (RLuc) reporter strain of HCV (JcR2A; Figure 2A). Eight of the 26 targets showed a significant reduction in HCV infection of Huh-7.5 cells upon RNAi. HIP1R, a previously reported HCV cofactor, also decreased HCV infectivity but did not meet our statistical significance criteria (Figure 2B; Table S5). *CD81*-targeting siRNAs served as positive control and reduced HCV infectivity more than 5-fold. None of the candidate targeting or scrambled siRNAs were cytotoxic or altered cell proliferation. Cystatin A (CSTA), a desmosomal regulator, dissociated almost completely from CD81 upon virus binding (Figures 1B and 1C), and its silencing led to a significant increase in HCV infectivity (Figure 2B).

Here, we chose to concentrate on the eight transient CD81 interaction partners, which reduced HCV infection when silenced (Figure 2B). Transcript levels of six of the eight targets were reduced to 25% or less of scrambled siRNA controls (Figure S2A). The six putative HCV host factors are SRFBP1, barrier-to-autointegration factor (BANF1), myosin-9 (MYH9), spectrin beta chain, non-erythrocytic 1 (SPTBN1), calpactin I light chain (S100A10), and poly [ADP-ribose] polymerase 1 (PARP1) (Table S6). Of all tested transient CD81 interactors, SRFBP1 showed the strongest reduction in HCV infectivity upon knockdown (z score [SRFBP1]: −6.3; z score [CD81]: −5.8). In summary, we found that at least six of the 26 tested transient CD81 interactors promote HCV infection with a clear bias for CD81 associating (five) over dissociating (one) factors (Figures 2C and S2B).

SRFBP1 Is Expressed in the Liver and Required for an Early Step in HCV Infection

SRFBP1 emerged as prime candidate for in-depth characterization as an HCV entry factor because the protein showed the strongest inhibition of HCV infection when silenced. We first quantified *SRFBP1* mRNA in primary hepatocytes from resection specimens of five HCV-negative donors and observed an up to 6-fold higher *SRFBP1* expression level than in Huh-7.5 cells (Figure 3A). Importantly, *SRFBP1* mRNA and protein levels correlated strongly (Figures S3A and S3B). The observed differences in *SRFBP1* expression led us to examine whether endogenous SRFBP1 levels were limiting HCV infection in hepatoma cells. When overexpressing SRFBP1 in Huh-7.5 cells, we observed a dose-dependent 2- to 3-fold increase in HCV infectivity (Figure 3B). Conversely, when silencing *SRFBP1* in primary hepatocytes, we observed a 4-fold decrease in HCV infectivity (Figure S3C). Collectively, this suggests that low SRFBP1 expression could contribute to the limited infectivity in current HCV cell culture models.

Next, we asked which step in the HCV life cycle requires SRFBP1. First, we confirmed that infectivity of incoming virus was impaired in *SRFBP1*-silenced hepatoma cells. A pool of three *SRFBP1*-targeting siRNAs and three individual siRNAs (nt96, nt394, and nt1038) reduced SRFBP1 protein expression and resulted in an up to 4-fold reduction in HCV infectivity (Figure 3C). *CD81*-silenced cells showed 5-fold decreased CD81 surface expression and a 10-fold reduction in infectivity (Figures 3C and S4A). We next excluded off-target effects of *SRFBP1* siRNA nt394 by complementing *SRFBP1*-silenced cells with a siRNA-resistant *SRFBP1* variant (Figure 3D). Taken together, silencing of *SRFBP1* led to a decrease in HCV susceptibility, and this phenotype could be rescued by *SRFBP1* complementation.

The association of SRFBP1 with the HCV entry factor CD81 suggested a role in HCV entry or an early post-entry event. Our infectivity readout at 48 hr post-HCV inoculation determined accumulative effects of virus entry, translation, replication, and spread (Gerold and Pietschmann, 2014). Thus, we next sought to exclude that SRFBP1 would affect HCV translation or replication. When silencing *SRFBP1* (nt394) in cells actively replicating HCV, we observed no impairment of replication and RLuc reporter translation at 48 or 72 hr post-RNAi. In stark contrast, silencing the known replication host factor *phosphatidyl inositol 4 kinase 3 alpha* (*PI4KIIIalpha*) reduced replication to background levels (Figure 3E, upper panel) (Berger et al., 2009; Reiss et al., 2011). Neither knockdown of *SRFBP1* nor of *PI4KIIIalpha* affected cell viability or proliferation (Figure 3E, middle panel). To address a possible role of SRFBP1 in assembly, release, and spread of HCV, we collected supernatants from HCV-replicating cells at

Figure 1. High-Resolution Quantitative MS Reveals Transient HCV Entry Factor Interactions

(A) Outline of the virus entry interaction proteomics procedure.

(B) CD81 interactome upon HCV exposure. Depicted are the mean $\log_2$ SILAC ratios of CD81-interacting proteins in HCV versus mock-treated samples from forward (y axis) and reverse experiments (x axis). Reverse label ratios are inverted, so that a positive correlation indicates reproducible interaction upon label swap. Significant (FDR < 5%) outliers are colored in red (CD81-associating proteins) and blue (CD81-dissociating proteins). Infinite ratio, interaction partners exclusively found in the presence of HCV. n.d., not quantified in either forward or reverse experiment.

(C) SILAC $\log_2$ ratios for each of the 13 CD81-associating and 13 CD81-dissociating factors. Shown are means ± SEM of four biological replicates with inverted reverse label ratios.

(D and E) Enrichment of Gene Ontology cellular component (GOCC) and molecular function (GOMF) annotations.

(F) Functional map of host factors transiently interacting with the HCV receptor CD81 during virus entry. Functional clusters (white boxes) and previously reported interactions (bold lines) of the here identified transient CD81-binding partners are depicted. We assigned individual proteins to the highest scoring DAVID cluster. Yellow lines between genes of different clusters indicate high-confidence (>0.9) STRING interactions. Within a functional annotation cluster, also lower confidence (>0.35) STRING interactions are shown. Proteins are placed in their predominant cellular location; SRFBP1 is shown twice as it localizes to nucleus and cytoplasm. The box size indicates the degree of CD81 association or dissociation upon HCV binding. Associating factors (red) and dissociating factors (blue) are shown. See also Figure S1 and Tables S1 and S2–S4.

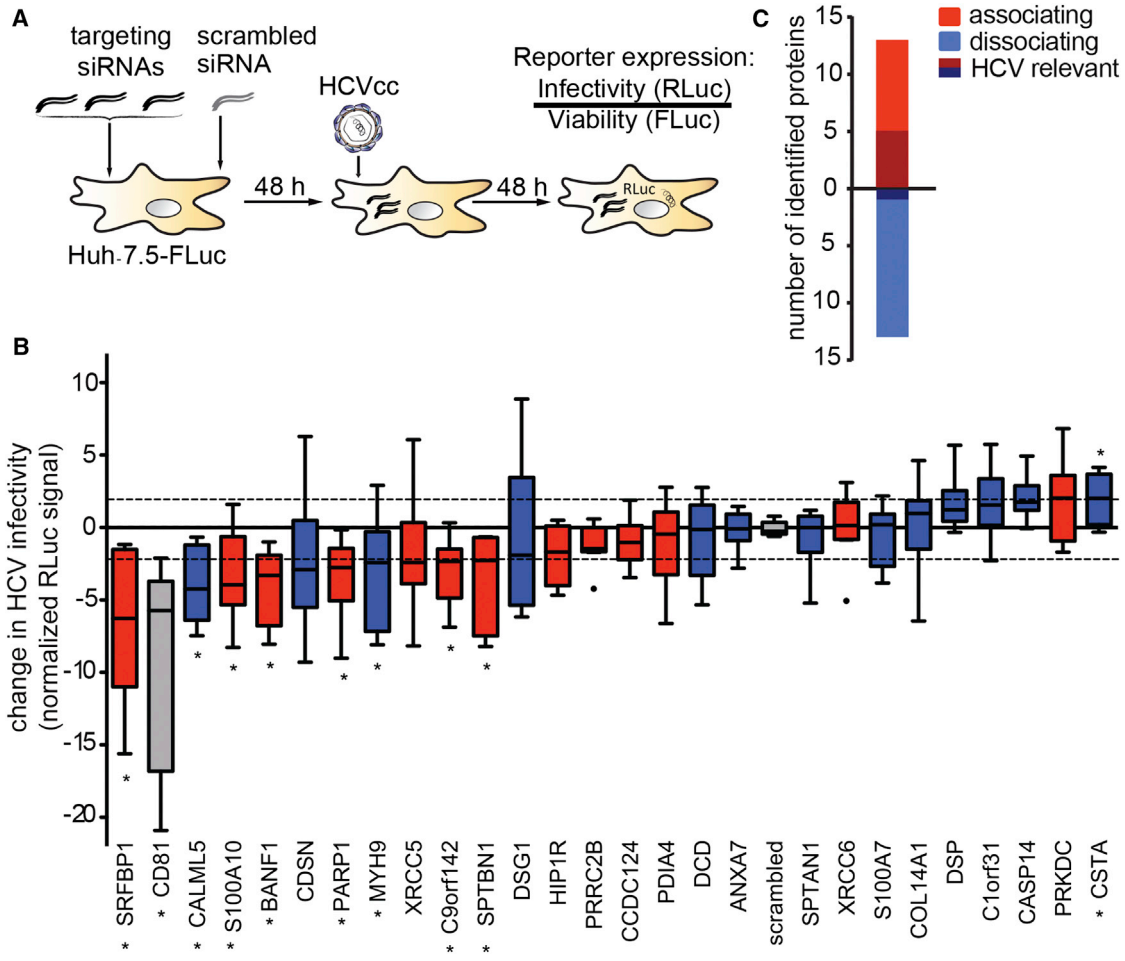

Figure 2. A Subset of CD81 Interaction Partners Is Required for HCV Infection

(A) Outline of the RNAi screen on transient CD81 interaction partners relevant for HCV infection.

(B) Functional RNAi follow-up screen on 26 selected transient CD81 interaction partners identifies nine putative host factors. We silenced the indicated transcript with a pool of three siRNAs in Huh-7.5 FLuc cells, infected 48 hr later with *Renilla* luciferase reporter HCV (JcR2A), and determined cell viability and HCV infectivity 48 hpi. Shown is the RLuc signal after normalization for cell viability and plate effects. Eight siRNA pools significantly decreased and one increased HCV infectivity ($p \leq 0.05$; abs [z score] ≥ 2; *). Associating factors (red), dissociating factors (blue), CD81 and scrambled controls (gray) are shown. Box and whisker plot of nine biological replicates is shown.

(C) The combined SILAC co-IP RNAi strategy reveals a bias for CD81-associating factors to act as HCV host factors. Out of 26 HCV-dependent CD81-binding partners, six decreased HCV infectivity upon RNAi with a minimum transcript reduction of 75% (shaded color). See also Figure S2 and Tables S5 and S6.

48 or 72 hr post-siRNA transfection and infected naive Huh-7.5 cells. *SRFBP1* silencing did not alter the released infectivity, whereas *apolipoprotein E* (*APOE*) silencing expectedly reduced the released infectivity to 40% (Figure 3E, lower panel) (Chang et al., 2007). Taken together, *SRFBP1* silencing rendered cells less susceptible to HCV without altering replication or spread of the virus to naive cells.

SRFBP1 Colocalizes with CD81 without Affecting HCV Receptor Surface Expression

In light of our finding that SRFBP1 plays a role early during HCV infection, we investigated whether SRFBP1 colocalizes with established HCV entry factors in resting cells. Whereas SRFBP1 only weakly colocalized with CLDN1, OCLN, or SR-BI (Pearson's coefficient < 0.2), a fraction of the protein colocalized with CD81 (Pearson's coefficient 0.4). In particular, SRFBP1 and CD81 signals overlapped in perinuclear regions and in the cell periphery, where we observed a punctate, vesicular staining. We further observed a weak colocalization with the membrane marker wheat germ agglutinin (WGA) (Pearson's coefficient 0.3; Figures 4A and 4B).

Next, we sought to exclude that SRFBP1 acts as a chaperone for CD81, CLDN1, OCLN, and SR-BI. In adipocytes, SRFBP1 is required for expression of the insulin-responsive glucose transporter type 4 (GLUT4) and for shuttling of GLUT4 to the plasma membrane (Lisinski et al., 2006). In contrast, we did not observe SRFBP1 colocalization with GLUT4 in hepatoma cells (Figures 4A and 4B). In line with these observations, *SRFBP1* silencing in hepatoma cells did not alter surface levels of CD81, CLDN1, or SR-BI, whereas silencing of *CD81* and *CLDN1* reduced

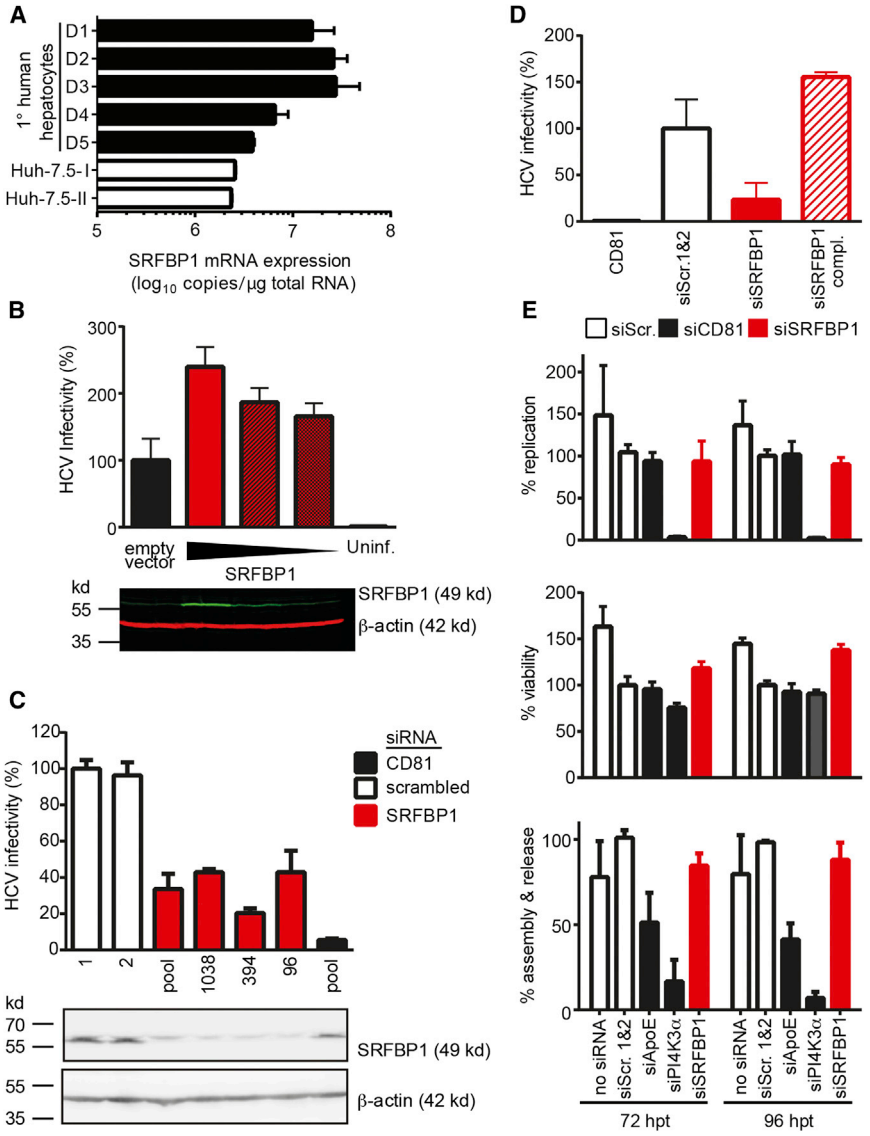

Figure 3. The CD81-Binding Partner SRFBP1 Is Expressed in Human Liver and Required for HCV Infection

(A) *SRFBP1* transcript levels in primary human hepatocytes are up to 6-fold higher than in Huh-7.5 cells. Absolute transcript numbers of *SRFBP1* in hepatocytes from five donors (D1–D5) and in two independent passages of human hepatoma cells (Huh-7.5) were determined in technical triplicates and displayed as mean + SD.

(B) HCV (JcR2A) infectivity increases in a dose-dependent manner in Huh-7.5 FLuc cells upon overexpression of full-length *SRFBP1*. Cells were transduced with lentiviruses encoding *SRFBP1* or a blasticidin resistance gene (empty vector), 72 hr later infected with HCV, and infectivity measured 48 hpi by luciferase assay. Immunoblot analysis of lysates 72 post-transduction shows dose-dependent SRFBP1 overexpression (green). Actin served as loading control (red). The immunoblot is representative of three biological replicates.

(C) HCV (JcR2A) infectivity is reduced in Huh-7.5 FLuc cells 48 hp silencing of *SRFBP1* or *CD81*. We used a pool of three siRNAs or individual siRNAs targeting the indicated ORF position and measured infectivity at 48 hpi by luciferase assay. Two scrambled siRNAs (1 and 2) served as controls. Immunoblot analysis confirms reduced SRFBP1 protein levels 48 hp RNAi. Mean + SD of three technical replicates are shown. Infectivity data and immunoblot are representative of three biological replicates.

(D) Lentiviral transduction with siRNA-resistant *SRFBP1* rescues HCV infection in *SRFBP1*-silenced Huh-7.5 FLuc cells. Cells were transfected with siRNAs (*SRFBP1*: siRNA 394), 24 hr later transduced with blasticidin resistance gene encoding lentivirus (siSRFBP1) or siRNA-resistant *SRFBP1* encoding lentivirus (siSRFBP1 compl.), and 24 hr later infected with HCV (JcR2A). Infectivity at 48 hpi measured by luciferase assay is shown.

(E) SRFBP1 is dispensable for HCV replication, assembly, and release. Huh-7.5 FLuc cells were transfected with genomic HCV RNA (JcR2A) and the indicated gene silenced 5 hr later (*SRFBP1*: siRNA 394). At 72 and 96 hp transfection (hpt), supernatants were harvested, cells lysed, and replication efficiency in lysates measured by luciferase assay (upper panel). Viability of HCV-replicating cells upon RNAi was determined using the cellular FLuc reporter at 72 or 96 hpt (middle panel). Supernatants from HCV-transfected and SRFBP1-silenced cells were titrated on naive Huh-7.5 cells to determine virus particle assembly and release rates (bottom panel). Values were normalized to a scrambled siRNA control. Unless stated otherwise, all experiments are displayed as mean + SD of three independent biological replicates each performed in technical triplicates. See also Figure S3.

surface expression of the respective protein (Figures 4C and S4A–S4C). Due to a lack of antibodies targeting the OCLN ectodomain, we addressed OCLN expression after knockdown by immunofluorescence and immunoblot. Total protein levels and plasma membrane expression of OCLN were similar in Huh-7.5 with or without *SRFBP1* knockdown (Figure 4D; data not shown). Similarly, transcript levels of the HCV entry cofactors EGFR and Niemann-Pick C1-like protein 1 (NPC1L1) (Sainz et al., 2012) remained unaffected by *SRFBP1* silencing (Figure S4D). Taken together, our data exclude that SRFBP1 acts as chaperone or transcriptional regulator of one of the previously characterized HCV entry factors.

SRFBP1 Partially Localizes to CD81-Positive Endosomes and Is Further Recruited to CD81 upon HCV Glycoprotein Exposure

To better visualize where and when during the HCV entry process SRFBP1 comes into play, we performed additional colocalization studies. We detected SRFBP1 in vesicular structures in the cell periphery, in perinuclear regions, and in heterochromatin regions of the nucleus. The nuclear localization of SRFBP1 is consistent with its transcription factor function described in cardiomyocytes (Zhang et al., 2004). Perinuclear SRFBP1 signals colocalized with the cytosolic trans-GOLGI marker p230 (Pearson's correlation coefficient 0.4). The punctate, vesicular pattern

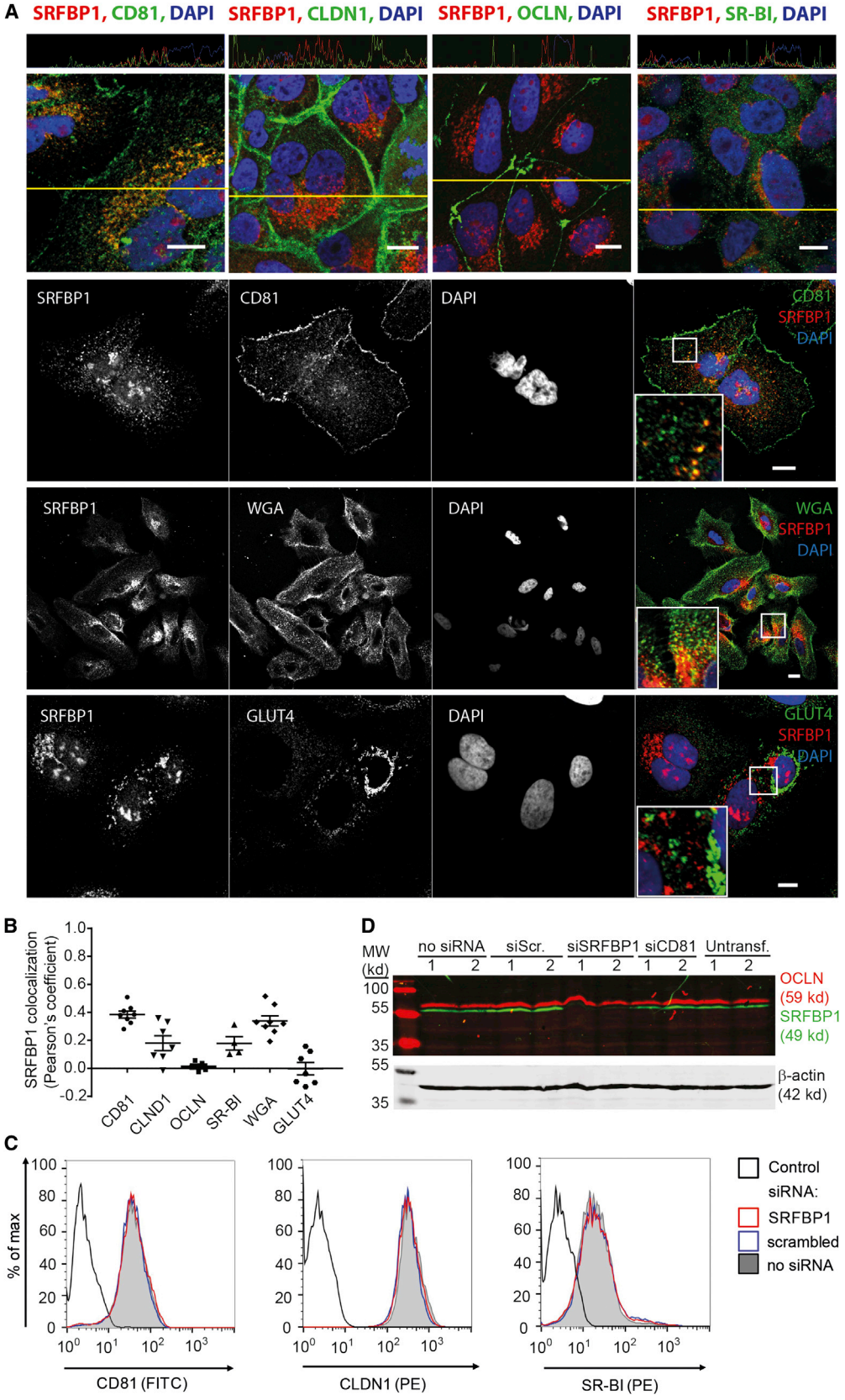

(legend on next page)

of SRFBP1 in the cell periphery weakly stained positive for the endosomal markers EEA and LAMP1, as well as for F and G actin (Figures 5A and 5B). To achieve more-sensitive visualization of endosomal compartments, we transfected EGFP-Rab fusion proteins (Nielsen et al., 1999) into Huh-7.5 cells. We found overlapping signals for SRFBP1 and CD81 at Rab5-positive early and late endosomes (Figures 5C and 5D). In favor of a role for SRFBP1 early during HCV infection, SRFBP1 did not reside in HCV replication or assembly compartments as shown by co-staining with the p body marker DDX6, the stress granule marker ataxin-1, and the lipid droplet dye oil red O (Figures S5A and S5C).

Next, we asked whether SRFBP1 could interact with intracellular membranes. SRFBP1 has no transmembrane domains, but we predicted two weak amphipathic helices at the N terminus of the protein (http://npsa-pbil.ibcp.fr/cgi-bin/npsa_automat.pl?page=/NPSA/npsa_amphipaseek.html; Sapay et al., 2006). In-depth analysis revealed that the putative helix at aa108 has a five-amino-acid hydrophobic side (FLLVI) flanked by lysine residues (http://heliquest.ipmc.cnrs.fr; Gautier et al., 2008). Moreover, two cysteine residues could serve as palmitoylation sites (Figure 5E). To confirm that a fraction of SRFBP1 is membrane associated, we performed membrane-flotation assays. In accordance with our prediction, a subfraction of endogenous SRFBP1 resided in the upper, membrane-associated gradient fractions (Figure 5F). As expected, CLDN1 and GAPDH resided in the upper and lower fractions, respectively. After solubilization of membranes using Triton X-100, we found endogenous SRFB1 exclusively in the soluble lower fractions and the CLDN1 control shifted partially to these fractions. Interestingly, a mycDDK-tagged overexpression construct of SRFBP1 resided in cytosolic fractions, suggesting that the soluble tag impaired membrane association of SRFBP1. Our analysis indicates that a fraction of SRFBP1 can associate with cellular membranes presumably through a weak amphipathic helix.

To test for relocalization of SRFBP1 during the HCV entry process, we exposed Huh-7.5 cells to purified ectodomain of the HCV E2 glycoprotein (eE2). This resulted in an increased colocalization of SRFBP1 and CD81 (Pearson's correlation coefficient 0.5), which could be reverted when coadministering an E2 blocking antibody (Figures 5G and 5H). Notably, we observed a similar recruitment of SRFBP1 to CD81-positive compartments in primary hepatocytes after eE2 exposure (Figures S5B and S5D) and in hepatoma cells after HCV exposure (Figure S5E). In summary, our data suggest that SRFBP1 partially resides at intracellular membranes in human hepatoma cells and that HCV glycoprotein exposure promotes colocalization of SRFBP1 and CD81.

SRFBP1, a Pan-genotypic and HCV-Specific Host Entry Factor

Next, we tested whether SRFBP1 also supports infection with other enveloped viruses. In Huh-7.5 cells, *SRFBP1* silencing neither reduced infectivity of vesicular stomatitis virus (VSV) or of human coronavirus 229E (Figures 6A and 6B), hinting that SRFBP1 is an HCV-specific host factor.

To further elucidate how SRFBP1 aids early HCV infection, we experimentally addressed HCV translation, replication complex formation, and membrane fusion. Using a bicistronic HCV IRES-driven translation reporter, we excluded a role for SRFBP1 in viral genome translation (Figures 6C, 6D, S6A, and S6B). Replication complex formation of subgenomic and full-length HCV replicons similarly remained unaltered upon *SRFBP1* silencing (Figures 6E, S6C, and S6D). In line with this observation, SRFBP1 did not colocalize with the HCV protein NS5A (Pearson's coefficient < 0.2; Figures S6E and S6F). We next induced HCV fusion at the plasma membrane by a low-pH wash and by concomitantly blocking endosomal acidification. In this assay, HCV enters cells by fusion at the plasma membrane or at the limiting endosomal membrane before acidification (Figure 6F). As expected, *CD81* silencing led to a 5-fold reduced HCV infectivity, as CD81 interactions prime the HCV glycoproteins for membrane fusion. Notably, silencing of *SRFBP1* reduced HCV infection by 3-fold, indicating that SRFBP1 functions in cell entry steps other than the acidification of endosomes. In confirmation of our assay setup, human coronavirus fusion at the plasma membrane was independent of pH, whereas VSV required a low-pH wash. Both coronavirus and VSV infectivity remained unaffected by *SRFBP1* or *CD81* silencing in this bypass assay (Figures S6G and S6H). Taken together, our data show that SRFBP1 is aiding an early step in HCV infection even when viral envelope fusion is artificially induced at the plasma membrane.

To pinpoint the requirements of the virus particle toward SRFBP1 usage, we tested whether lentiviral pseudoparticles decorated with HCV glycoproteins depend on SRFBP1. Interestingly, lentiviral pseudotypes for HCV genotype 1 (H77) and 2 (J6; Hsu et al., 2003) transduced *SRFBP1*-silenced cells efficiently. *CD81* silencing reduced HCV pseudoparticle entry 10-fold, whereas none of the tested conditions affected control pseudoparticles carrying VSV glycoproteins (Figure 6G). Thus, SRFBP1 does not affect receptor binding but instead supports an

Figure 4. SRFBP1 Colocalizes with CD81 without Affecting Entry Factor Surface Expression

(A) SRFBP1 partially colocalizes with CD81 and the membrane marker WGA but only weakly with CLDN1, OCLN, SR-BI, and GLUT4. Huh-7.5 cells were stained with Alexa-conjugated membrane marker WGA (panel 3) for 1 min or left unstained (panels 1, 2, and 4), fixed, permeabilized, and stained for SRFBP1 and the indicated protein. Nuclei were stained with DAPI. Colocalization across a section (yellow line in panel 1) is depicted above the respective image. Representative confocal images; insert 2.2-fold magnification; scale bars 10 μm.

(B) Pearson's correlation coefficient for SRFBP1 and the indicated cellular protein or the membrane marker WGA calculated by intensity correlation analysis. Each symbol represents an individual frame; horizontal lines indicate the mean ± SEM.

(C) *SRFBP1*-silenced cells (siRNA 394) express CD81, CLDN1, and SR-BI at the plasma membrane. Surface expression of CD81, CLDN1, and SR-BI on Huh-7.5 cells was analyzed 48 hpt with the indicated siRNAs. Cells were stained with antibodies against HCV entry factors followed by flow cytometric analysis of 10,000 cells per sample. For quantification and additional controls, see Figure S4. Control is directly conjugated isotype antibody (histogram 1) or secondary antibody only (histograms 2 and 3).

(D) OCLN expression levels are stable after *SRFBP1* silencing (siRNA 394). Immunoblot analysis of OCLN (red) and SRFBP1 (green) after siRNA mediated silencing for 48 hr is shown. Actin served as loading control. Data are representative of at least three independent experiments. See also Figure S4.

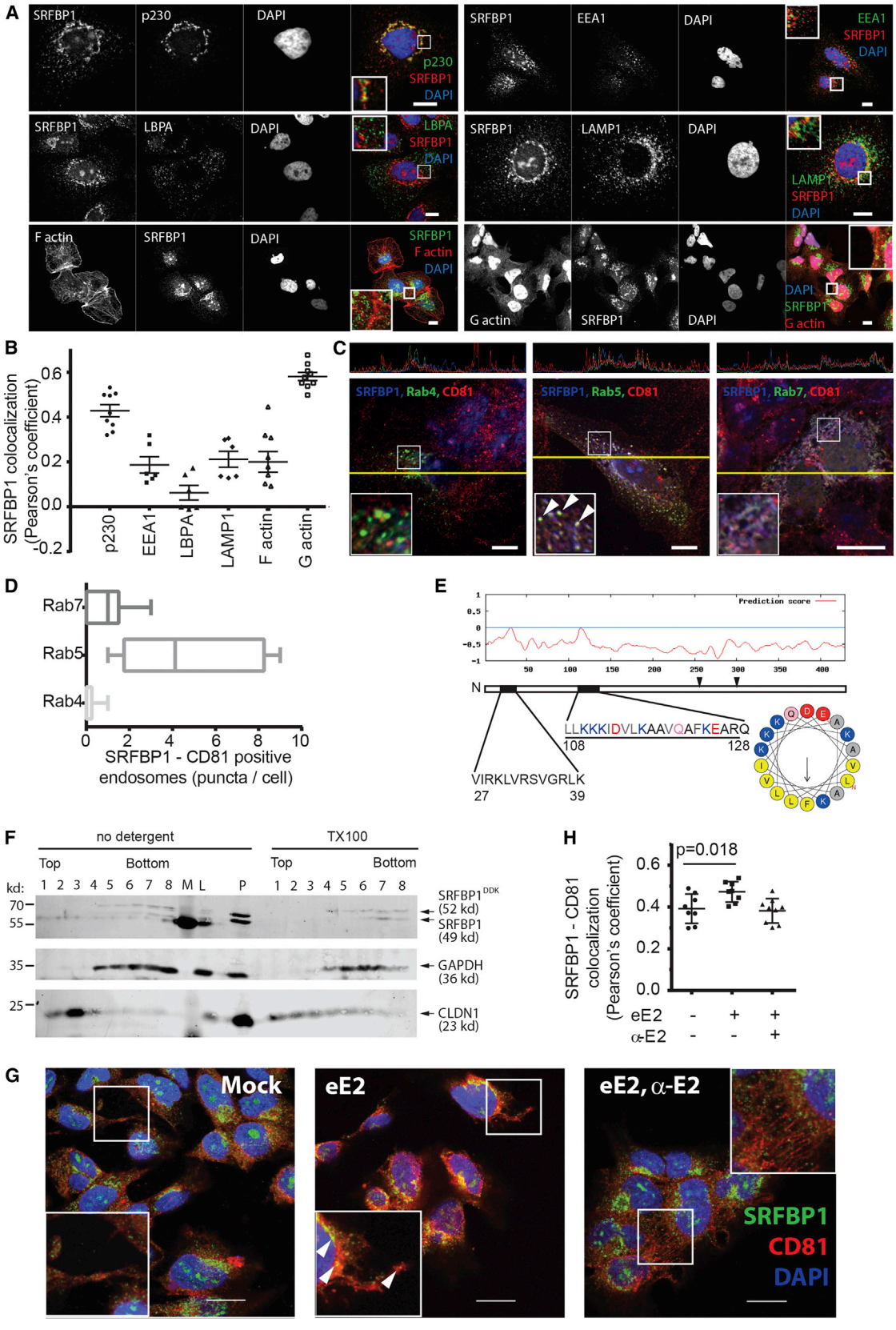

(legend on next page)

infection step not reflected by HCV pseudoparticles. Furthermore, SRFBP1 did not influence lentiviral transduction. Collectively, our results show that SRFBP1 is dispensable for lentiviral pseudotype, VSV, and coronavirus infection but required to render cells fully susceptible to HCV.

Lastly, we addressed whether, in addition to cell culture HCV of genotype 2a, other clinically relevant HCV genotypes require SRFBP1 for efficient penetration. *SRFBP1* interference reduced infectivity of chimeric viruses displaying the glycoproteins of either one of the seven HCV genotypes to a similar degree (Figure 6H). Thus, through quantitative interaction proteomics, we could identify six putative HCV host factors and, in particular, SRFBP1 as a pan-genotypic entry factor for HCV.

DISCUSSION

Our results demonstrate that quantitative interaction proteomics combined with RNAi provides a valuable approach to study host-pathogen interactions. Quantitative MS provides direct information on protein-protein interactions and interaction strength upon perturbation of a cellular system. Here, we developed a SILAC co-IP strategy to identify host factors, which transiently interact with the HCV receptor CD81. The data set allowed generation of a weighted virus entry network and identification of cellular processes during entry.

Among the identified 26 transient interaction partners of CD81, four (DSG1, CSTA, DSP, and CDSN) are integral parts of cellular junctions, in particular desmosomes. These proteins dissociated from CD81 during virus entry, suggesting that the virus receptor complex leaves desmosomal membrane compartments during uptake. The second enriched cluster of Ca^{2+}-binding proteins (CALML5, S100A7, and S100A10) could contribute to the reported Ca^{2+}-dependent ER stress and deregulation of Ca^{2+} homeostasis induced by HCV (Benali-Furet et al., 2005; Piccoli et al., 2009). Here, we focused on CD81 interaction partners, which support HCV infection, and found that these comprise at least 23% of the 26 interactors. The putative HCV host factors are SRFBP1, S100A10, BANF1, PARP1, MYH9, and SPTBN1 (Table S6). The latter two guide cytoskeleton movement at the plasma membrane, which is in line with the reported membrane "surfing" of HCV (Brazzoli et al., 2008). S100A10 is a component of the annexin 2 heterotetramer and regulates membrane organization and endocytosis. We conclude that quantitative proteomics can identify functional virus-host cell interactions.

Several HCV host factors described in this study play a role in the life cycle of other enveloped viruses. MYH9 (also known as myosin IIA) regulates Kaposi's sarcoma-associated herpesvirus macropinocytosis (Valiya Veettil et al., 2010). S100A10 is phosphorylated by the HCV host factor EGFR (Lupberger et al., 2011) and promotes uptake of papillomaviruses upon EGFR-driven phosphorylation (Dziduszko and Ozbun, 2013; Woodham et al., 2012). The protein is also thought to be a cofactor for entry of HIV-1, cytomegalovirus, and respiratory syncytial virus (Ma et al., 2004; Malhotra et al., 2003; Raynor et al., 1999). BANF1 is involved in nuclear DNA repair and HIV-1 genome integration (Chen and Engelman, 1998) and senses vaccinia virus genomes in the cytoplasm (Ibrahim et al., 2011). PARP1 has poly(ADP-ribosyl)ation activity and is sequestered to the cytoplasm during HIV-1 and Sindbis virus infection (Muthumani et al., 2006; Park and Griffin, 2009). Hence, we identified six putative HCV host factors, which are linked to known HCV entry machineries, e.g., clathrin-mediated endocytosis and EGFR signaling, or have a reported role in infection or sensing of other enveloped viruses.

SRFBP1 emerged as prime candidate for follow up and proof of principle analysis as the protein had the strongest RNAi phenotype in our screen. The protein promotes plasma membrane expression of GLUT4 in adipocytes (Lisinski et al., 2006), associates with actin, and has transcription factor activity in cardiomyocytes (Zhang et al., 2004, 2014). In this study, we identify SRFBP1 as transient binding partner of the HCV receptor CD81 in human hepatoma cells. Our results demonstrate that SRFBP1 is required for productive uptake of HCV without affecting expression or membrane localization of known HCV entry factors. We further show that primary hepatocytes

Figure 5. A Pool of SRFBP1 Localizes to CD81 on Endosomes and Is Recruited to CD81 upon HCV Glycoprotein Exposure

(A) SRFBP1 localizes to the trans-GOLGI, endosomes, and actin. Huh-7.5 cells were stained for SRFBP1; the trans-GOLGI marker p230; and the endosomal markers EEA1, LBPA, and LAMP1 as described in Figure 4A. F and G actin were stained with Alexa-conjugated phalloidin and DNase I, respectively.

(B) Pearson's correlation coefficient for SRFBP1 and indicated cellular proteins calculated by intensity correlation analysis. Each symbol represents an individual frame; horizontal lines indicate the mean ± SEM.

(C) SRFBP1 localizes to CD81 on endosomes. Huh-7.5 cells were transfected with expression plasmids for EGFP-Rab4, -Rab5, and -Rab7 and stained for SRFBP1 and CD81. Colocalization of SRFBP1, CD81, and Rab proteins across a section (yellow line) is depicted in the upper panels. Arrowheads indicate colocalization.

(D) SRFBP1 and CD81 colocalize at early endosomes. Quantification of SRFBP1, CD81, and Rab triple-positive puncta is shown. Box and whisker plot showing median, minimum, and maximum values from six independent frames.

(E) Bioinformatics prediction of two weak amphipathic helices for SRFBP1 (black bars) with the second helix (aas 108–128) showing a small hydrophobic face of five amino acids (FLLVI). The hydrophobic face is highlighted in light gray in the primary sequence and in yellow in the helix model. Two cysteine residues (aa 254 and aa 300), which could serve as palmitoylation sites, are indicated by arrowheads.

(F) Membrane flotation assay suggests membrane association of SRFBP1. Huh-7.5 cells were transduced with mycDDK-tagged SRFBP1, 48 hr later lysed in hypotonic buffer, and analyzed by Nycodenz gradient ultracentrifugation followed by immunoblot analysis against SRFBP1, GAPDH, and CLDN1. TX-100-treated lysates served as solubilization control. L, precleared lysate; M, marker; P, pellet after lysate preclearing. One out of three independent experiments is shown.

(G) Exposure to soluble HCV glycoprotein (eE2) increases SRFBP1-CD81 colocalization in Huh-7.5 cells. Cells were incubated with eE2, with eE2 and an E2 blocking antibody (α-E2), or with PBS (mock) for 15 min; fixed; and stained for SRFBP1 and CD81 as described in Figure 4A. Arrowheads indicate colocalization.

(H) Pearson's correlation coefficient for SRFBP1 and CD81 calculated by intensity correlation analysis. Each symbol represents an individual frame; horizontal lines indicate the mean ± SEM; p value is indicated.

Representative images; inserts show magnification; scale bars 10 μm (A and C) and 20 μm (G). See also Figure S5.

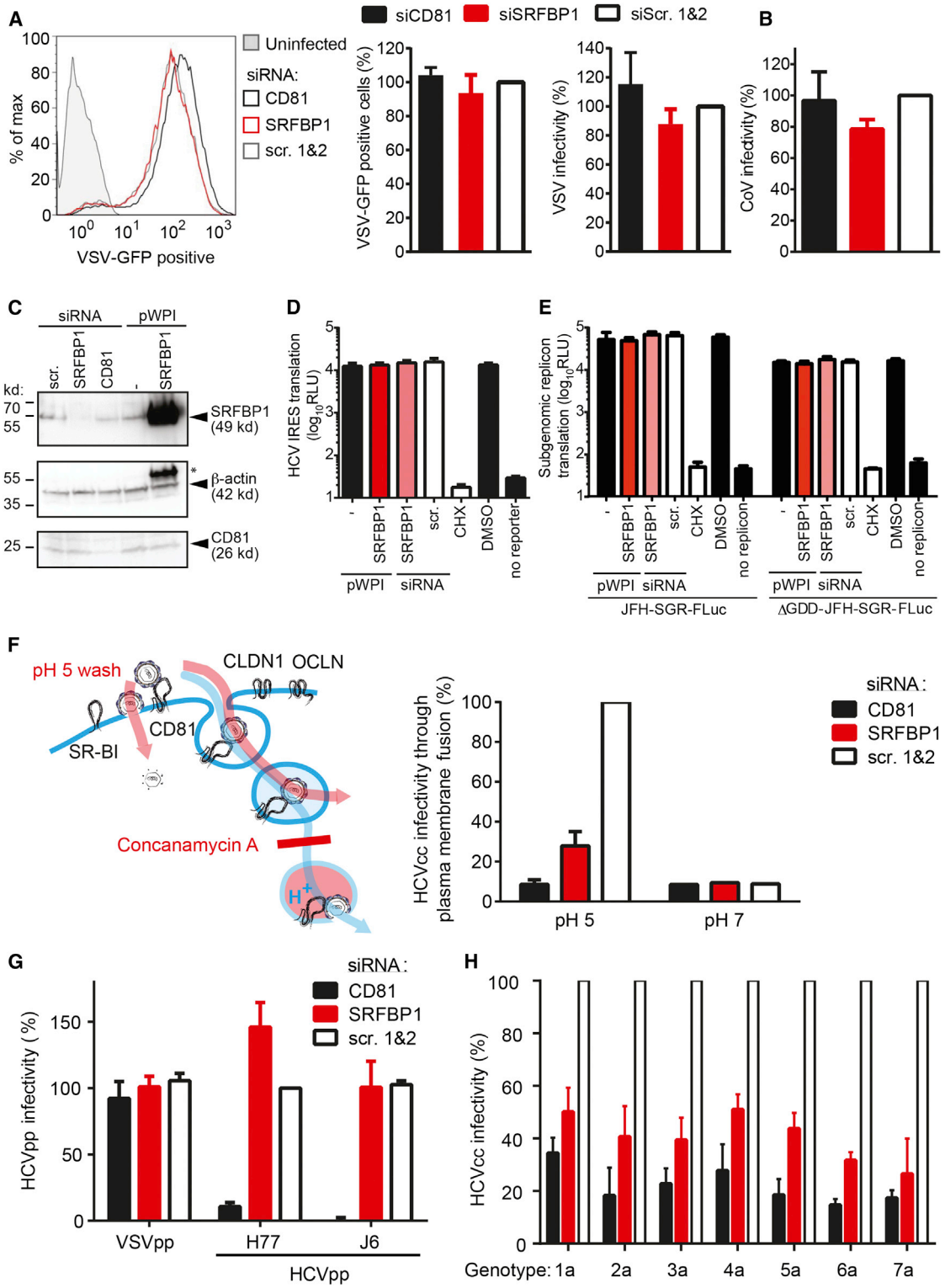

Figure 6. SRFBP1 Is a Pan-genotypic and HCV-Specific Host Entry Factor

(A) SRFBP1 is dispensable for VSV infection. *SRFBP1*-silenced Huh-7.5 cells were infected with VSV*M_Q (MOI 0.1) and analyzed for GFP expression by flow cytometry 20 hpi. Histogram is representative of biological triplicates (left panel). Quantification of VSV*M_Q infectivity 20 hpi in *SRFBP1*-silenced cells is determined as percentage of GFP-positive cells (middle panel) or by normalization of the mean fluorescence intensity (MFI) of VSV-infected *SRFBP1*- or *CD81*-silenced cells to MFI of scrambled siRNA-transfected cells (right panel).

(legend continued on next page)

express up to 6-fold higher transcript levels of SRFBP1 than hepatoma cells, in which SRFBP1 expression seems to limit HCV infectivity. Thus, SRFBP1 might play a critical role in HCV infection in patients.

Collectively, our data suggest that SRFBP1 is a bona fide entry factor for HCV (Figure 7). During the HCV entry pathway, SRFBP1 supports a step independent of receptor binding, clathrin-mediated endocytosis, and endosomal acidification. The latter three steps are reliably mimicked by lentiviral HCV pseudotypes, which enter cells independent of SRFBP1. The observed discrepancy between cell culture HCV and HCV pseudoparticles confirms other studies suggesting that HCV pseudoparticles cannot fully mimic the entry pathway of HCV (Sainz et al., 2012). This can be attributed either to the lower avidity of HCV pseudoparticles, which display a lower density of glycoproteins, to the lack of serum lipoprotein association of HCV pseudoparticles, or to the different nucleocapsid.

Here, we propose two possible modes of action of SRFBP1 during HCV entry. First, SRFBP1 could be involved in actin retrograde transport of HCV particles as observed by Coller et al. (2009). Such actin cortex remodeling is not induced by HCV pseudoparticles (Harris et al., 2013). Second, SRFBP1 might assist HCV uncoating or nucleocapsid transport, both of which are not reflected by the pseudoparticle system. Generally, SRFBP1 could be the missing link between HCV receptor binding and actin-dependent movement during HCV invasion. Indeed, we observed an interaction of SRFBP1 with G actin. Moreover, EGFR, Arp2/3, Rho GEFs, and Rho GTPases are reported upstream activators of the SRFBP1 protein family and at the same time support HCV entry (Brazzoli et al., 2008; Lupberger et al., 2011; Zona et al., 2013). Future studies including high-resolution imaging will be necessary to experimentally validate either model.

The endogenous function of cytoplasmic SRFBP1 is currently elusive. In rat cardiomyocytes, SRFBP1 localizes to actin fibers close to their attachment site to the cell cortex and *SRFBP1* overexpression leads to actin depolymerization (Zhang et al., 2014). This hints that SRFBP1 belongs to the class of myocardin-related transcription factor (MRTF) cofactors (Olson and Nordheim, 2010), which regulate actin polymerization by cycling between a G-actin-bound cytoplasmic state and a nuclear state. Concordantly, we found SRFBP1 in the nucleus and at cytoplasmic G actin in human hepatoma cells. Like other MRTF cofactors, SRFBP1 could regulate actin dynamics downstream of plasma membrane receptor signaling. In line with this, CD81 engagement by antibodies was recently reported to promote actin-dependent hepatoma spread (Brimacombe et al., 2014). Thus, HCV might exploit endogenous mechanisms of physical force generation to traffic during its entry.

Taken together, we established a combination of high-resolution MS, computational proteomics, and RNAi to elucidate receptor complex rearrangements during HCV entry. We believe that quantitative interaction proteomics is an attractive strategy to identify host factors of infectious agents. A particular strength lies in the unbiased identification of yet uncharacterized proteins as we demonstrate for SRFBP1, a protein with previously unknown function in hepatocytes. Moreover, interaction proteomics allows the identification of host factors, which are ubiquitously expressed, and are thus not accessible by genetic complementation screens. Similarly, host factors with essential endogenous function are poorly suited for stable knockdown or knockout screens and can readily be found by quantitative proteomics. Thus, the minimal system perturbation during the above-described workflow is a clear benefit over classical genetic screening methods. On the other hand, functional information on the identified host factors is limited to the interaction with a given virus receptor. A functional follow-up screen, as we describe here, is therefore critical to evaluate the protein interaction data. Consequently, interaction proteomics is a complementary method in the thus far genomics-oriented toolbox for systems virology (Law et al., 2013). As for other systems biology methods, interaction proteomics is not error free. Although detection limits for MS fingerprinting have increased tremendously in the past years (Cox and Mann, 2012), false negatives might arise depending on the affinity enrichment method used. False positive interactions could obviously arise after cell lysis

(B) SRFBP1 is dispensable for coronavirus infection. *SRFBP1*-silenced cells were infected with HCoV229E-luc (MOI 0.1) and RLuc activity in cell lysates measured 24 hpi. Infectivity relative to a scrambled siRNA control is shown.

(C) Immunoblot analysis of SRFBP1 and CD81 48 hp siRNA transfection. Huh-7.5 cells were transfected with siRNA or transduced with the indicated pWPI expression construct as in (A)–(H), 48 hr later lysed, and analyzed by immunoblot. Actin served as loading control. *, residual SRFBP1 signal.

(D) Bicistronic translational reporter assay with HCV IRES-driven RLuc and cap-dependent FLuc (see also Figures S6A and S6B). *SRFBP1* silencing and overexpression was performed as in (C), and 48 hr later, cells were transfected with translational reporter RNA. Eight hours after reporter transfection, luciferase activity in lysates was monitored.

(E) Early replication reporter assay using a subgenomic HCV genome expressing FLuc. *SRFBP1* silencing and overexpression was performed as in (C), and 48 hr later, JFH-SGR-FLuc RNA was transfected into cells; cells lysed after 8 hr; and luciferase activity monitored. A polymerase mutant JFH-SGR-FLuc replicon (ΔGDD) was used to assess translation of HCV genomes independent of de novo replication. See also Figures S6C and S6D for additional controls.

(F) SRFBP1 is required in a plasma membrane fusion assay of HCV infection. Huh-7.5 cells silenced for *SRFBP1* were pretreated with concanamycin A (5 nM; 1 hr) to block vacuolar type H^+-ATPases, incubated with HCV (JcR2A) for 2 hr at 4°C in the presence of concanamycin A, shifted to 37°C, and washed with a pH 5 or pH 7 buffer for 5 min. After incubation with concanamycin A for 4 hr, medium was changed and endosomal acidification independent infectivity measured at 48 hpi. See also Figures S6E and S6F for additional controls.

(G) Lentiviral pseudotypes infect Huh-7.5 cells independently of SRFBP1. Cells in which *SRFBP1* had been silenced (48 hr) were infected with HIV-1 pseudotypes encoding FLuc and displaying glycoproteins from HCV genotype 1 (H77), HCV genotype 2 (J6), VSV, or no glycoprotein. At 72 hpi, cells were lysed and FLuc activity measured. Infectivity was calculated by subtraction of background read for glycoprotein-free particles and relative to VSVG particles.

(H) Silencing of *SRFBP1* reduces infectivity of chimeric HCV viruses with glycoproteins from all seven genotypes. Huh-7.5 FLuc cells were subjected to siRNA-mediated silencing followed by infection with intergenotypic HCV chimeras (MOI 0.1) expressing RLuc. Forty-eight hours post-infection, infectivity was determined by RLuc activity measurement. Cells treated with *CD81* targeting or scrambled siRNAs served as controls. *SRFBP1*-targeting siRNA 394 was used in all experiments. Data from three to five biological replicates are displayed as mean + SD. See also Figure S6.

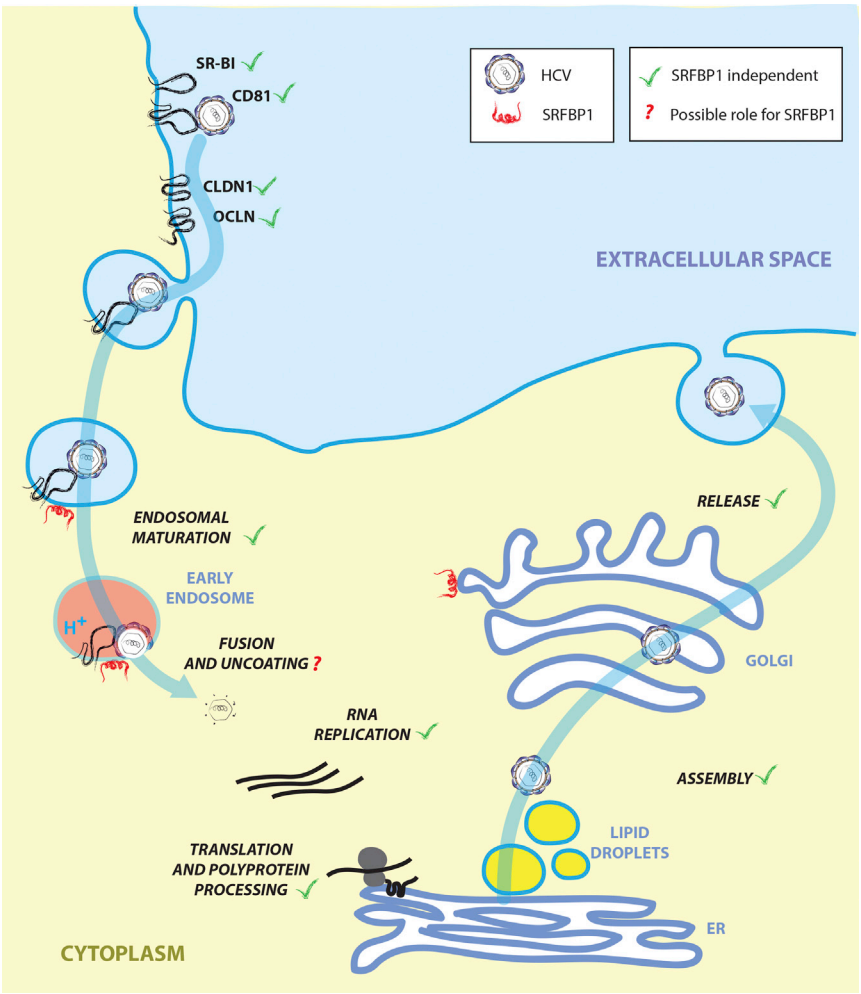

Figure 7. HCV Life Cycle and Possible Role for SRFBP1 during HCV Entry

Our data point toward a role for SRFBP1 in the last step of entry; i.e., nucleocapsid uncoating.

and disruption of cellular compartments, and thus, careful follow-up analysis is critical for the here-described methodology. Clearly, receptor interaction proteomics will not only allow the follow-up search for entry factors but can also reveal host factors involved in innate immune recognition or cellular perturbations triggered by the virus like, e.g., apoptosis (Figure S7). Given that co-IP proteomics reveals interconnectivity of pathogen receptors and host cofactors, we envision that the technique can spur the development of peptidomimetics or small molecules for therapeutic intervention of pathogen invasion (de Chassey et al., 2012).

EXPERIMENTAL PROCEDURES

SILAC Labeling and HCV Inoculation

Huh-7 cells were passaged eight times in light or heavy label media, i.e., Arg- and Lys-free DMEM (PAA Laboratories) supplemented with 2 mM L-glutamine, 1 mM pyruvate, 10% dialyzed FBS, 0.375% sodium bicarbonate, 48 μg/ml Arg (Arg-0, Arg-6, and Arg-10, respectively), and 73 μg/ml Lys (Lys-0 and Lys-8, respectively; Cambridge Isotope Labs). Confluent P150 cultures were incubated with J6/JFH clone 2 (MOI 10 after 1:5 dilution in serum-free label media) for 15 min at 37°C or treated in a similar manner with virus-free conditioned cell culture media processed in the same way as the HCV preparation (mock electroporation). One-step immunoprecipitations of membrane proteins were performed as detailed in the Supplemental Experimental Procedures. Experiments were conducted in four replicates (two heavy- and two light-labeled cultures per experimental condition).

MS Bioinformatics, Hierarchical Clustering, and Hit Scoring

Mass spectra were acquired and analyzed as described in the Supplemental Experimental Procedures. For each HCV and mock-treated SILAC pair with a given label combination, normalized ratios were calculated from the individual heavy and light peptide intensities as described in Cox and Mann (2008).

Transient protein interactions (i.e., regulated CD81 binding during HCV entry) were defined by differing significantly from the main distribution of steady-state interactors using significance B with a false discovery rate of 5% as described in Cox and Mann (2008). By this analysis, 55 proteins from a total of 778 proteins were identified, which grouped into 29 associating and 26 dissociating proteins (Table S1). Proteins were required to be significantly regulated in at least one experiment to be included for further analysis. To quantify proteins, which were only detected in one experimental condition (HCV or mock), we analyzed the total ion intensities for heavy and light peptides separately. We detected five proteins exclusively in HCV samples, four of which were liver expressed. No proteins were exclusively detected in mock samples.

Proteins significantly regulated upon HCV incubation were ranked by their fold change and only those with >2.1-fold change considered for further analysis. Forty-seven interaction partners of CD81 fulfilled this criterion. For functional follow up of CD81-binding proteins, we additionally filtered for expression in human liver and for subcellular localization. Proteins with lacking liver expression or strict ribosomal and nuclear localization were excluded from downstream analysis, resulting in 26 selected CD81-binding partners to be tested for their role in HCV infection.

The protein interactions from this publication have been submitted to the IMEx (http://www.imexconsortium.org) consortium through IntAct and assigned the identifier IM-24070 (Orchard et al., 2014).

RNAi Screen for HCV Host Factors and Bioinformatic Analysis

Huh-7.5 cells stably expressing *Firefly* luciferase (Huh-7.5 FLuc) were transfected with pools of three siRNAs against the 26 selected transient CD81 interaction partners (Ambion Silencer Select) and infected with the *Renilla* luciferase reporter virus JcR2A (MOI 0.1) as detailed in the Supplemental Experimental Procedures. The screen was performed nine times on Huh-7.5 FLuc cells of three independent passages. Normalization and statistical analysis was performed on a set of 34 targets total in R using the Bioconductor package RNAither (Rieber et al., 2009).

Cell lines, viruses, used reagents, and detailed methods are described in the Supplemental Experimental Procedures. Human samples were handled under oversight of the ethics committee of the Hannover Medical School.

SUPPLEMENTAL INFORMATION

Supplemental Information includes Supplemental Experimental Procedures, seven figures, and six tables and can be found with this article online at http://dx.doi.org/10.1016/j.celrep.2015.06.063.

AUTHOR CONTRIBUTIONS

G.G. designed experiments, performed experiments, evaluated and interpreted the data, and wrote the manuscript. F.M. designed and performed the mass spec analysis and assisted with writing the manuscript. J.B. and K.W. performed experiments. P.M.P. performed fusion assays. T.F.B. generated and provided monoclonal anti-SR-BI antibody. A.G.K. and J.M. provided purified eE2. F.W.V. isolated and provided primary hepatocytes. L.K. performed RNAi statistics. M.M. advised on quantitative mass spec analysis. C.M.R. and T.P. advised on experimental approaches, evaluated and interpreted the data, and assisted with writing the manuscript.

ACKNOWLEDGMENTS

We thank Takaji Wakita for the JFH1 isolate; Jens Bukh for intergenotypic chimeric HCV strains; Marino Zerial for Rab-GFP constructs; Dirk Lindemann for the pc.Z.VSV-G plasmid; Gert Zimmer for VSV*M_O; Volker Thiel for coronavirus 229E-Luc; Didier Trono for pWPI and pCMVdeltaR8.74 constructs; and Annie Cahour, Jean Dubuisson, and Yves Rouille for the pIRF construct. This work was supported by fellowships from the Human Frontier Science Program (LT-000048-2009), the German Academy of Science Leopoldina (LPDS 2009-9), the German Research Foundation (DFG; GE 2145/3-1), and the German Liver Foundation (S163/10073/2011; to G.G.). Grants from the Deutsche Forschungsgemeinschaft (SFB 900; project A6) and the Helmholtz Association SO-024 funded T.P. The work was also supported by US Public Health Service NIH grant R01 AI072613 (to C.M.R.), the Greenberg Medical Research Institute, and the Starr Foundation. C.M.R. has equity in Apath, LLC, which holds commercial licenses for the Huh-7.5 cell line and HCV cell culture system.

Received: August 29, 2014
Revised: May 18, 2015
Accepted: June 22, 2015
Published: July 23, 2015

REFERENCES

Benali-Furet, N.L., Chami, M., Houel, L., De Giorgi, F., Vernejoul, F., Lagorce, D., Buscail, L., Bartenschlager, R., Ichas, F., Rizzuto, R., and Paterlini-Bréchot, P. (2005). Hepatitis C virus core triggers apoptosis in liver cells by inducing ER stress and ER calcium depletion. Oncogene *24*, 4921–4933.

Berger, K.L., Cooper, J.D., Heaton, N.S., Yoon, R., Oakland, T.E., Jordan, T.X., Mateu, G., Grakoui, A., and Randall, G. (2009). Roles for endocytic trafficking and phosphatidylinositol 4-kinase III alpha in hepatitis C virus replication. Proc. Natl. Acad. Sci. USA *106*, 7577–7582.

Blanchard, E., Belouzard, S., Goueslain, L., Wakita, T., Dubuisson, J., Wychowski, C., and Rouillé, Y. (2006). Hepatitis C virus entry depends on clathrin-mediated endocytosis. J. Virol. *80*, 6964–6972.

Brazzoli, M., Bianchi, A., Filippini, S., Weiner, A., Zhu, Q., Pizza, M., and Crotta, S. (2008). CD81 is a central regulator of cellular events required for hepatitis C virus infection of human hepatocytes. J. Virol. *82*, 8316–8329.

Brimacombe, C.L., Wilson, G.K., Hübscher, S.G., McKeating, J.A., and Farquhar, M.J. (2014). A role for CD81 and hepatitis C virus in hepatoma mobility. Viruses *6*, 1454–1472.

Chang, K.S., Jiang, J., Cai, Z., and Luo, G. (2007). Human apolipoprotein e is required for infectivity and production of hepatitis C virus in cell culture. J. Virol. *81*, 13783–13793.

Charrin, S., Le Naour, F., Labas, V., Billard, M., Le Caer, J.P., Emile, J.F., Petit, M.A., Boucheix, C., and Rubinstein, E. (2003). EWI-2 is a new component of the tetraspanin web in hepatocytes and lymphoid cells. Biochem. J. *373*, 409–421.

Chen, H., and Engelman, A. (1998). The barrier-to-autointegration protein is a host factor for HIV type 1 integration. Proc. Natl. Acad. Sci. USA *95*, 15270–15274.

Coller, K.E., Berger, K.L., Heaton, N.S., Cooper, J.D., Yoon, R., and Randall, G. (2009). RNA interference and single particle tracking analysis of hepatitis C virus endocytosis. PLoS Pathog. *5*, e1000702.

Cox, J., and Mann, M. (2008). MaxQuant enables high peptide identification rates, individualized p.p.b.-range mass accuracies and proteome-wide protein quantification. Nat. Biotechnol. *26*, 1367–1372.

Cox, J., and Mann, M. (2012). 1D and 2D annotation enrichment: a statistical method integrating quantitative proteomics with complementary high-throughput data. BMC Bioinformatics *13* (*16*), S12.

de Chassey, B., Meyniel-Schicklin, L., Aublin-Gex, A., André, P., and Lotteau, V. (2012). New horizons for antiviral drug discovery from virus-host protein interaction networks. Curr Opin Virol *2*, 606–613.

Diao, J., Pantua, H., Ngu, H., Komuves, L., Diehl, L., Schaefer, G., and Kapadia, S.B. (2012). Hepatitis C virus induces epidermal growth factor receptor activation via CD81 binding for viral internalization and entry. J. Virol. *86*, 10935–10949.

Dziduszko, A., and Ozbun, M.A. (2013). Annexin A2 and S100A10 regulate human papillomavirus type 16 entry and intracellular trafficking in human keratinocytes. J. Virol. *87*, 7502–7515.

Evans, M.J., von Hahn, T., Tscherne, D.M., Syder, A.J., Panis, M., Wölk, B., Hatziioannou, T., McKeating, J.A., Bieniasz, P.D., and Rice, C.M. (2007). Claudin-1 is a hepatitis C virus co-receptor required for a late step in entry. Nature *446*, 801–805.

Farquhar, M.J., Hu, K., Harris, H.J., Davis, C., Brimacombe, C.L., Fletcher, S.J., Baumert, T.F., Rappoport, J.Z., Balfe, P., and McKeating, J.A. (2012). Hepatitis C virus induces CD81 and claudin-1 endocytosis. J. Virol. *86*, 4305–4316.

Gautier, R., Douguet, D., Antonny, B., and Drin, G. (2008). HELIQUEST: a web server to screen sequences with specific α-helical properties. Bioinformatics *24*, 2101–2102.

Gerold, G., and Pietschmann, T. (2014). The HCV life cycle: in vitro tissue culture systems and therapeutic targets. Dig. Dis. *32*, 525–537.

Gerold, G., and Rice, C.M. (2011). Locking out hepatitis C. Nat. Med. *17*, 542–544.

Gravitz, L. (2011). Introduction: a smouldering public-health crisis. Nature *474*, S2–S4.

Harris, H.J., Clerte, C., Farquhar, M.J., Goodall, M., Hu, K., Rassam, P., Dosset, P., Wilson, G.K., Balfe, P., Ijzendoorn, S.C., et al. (2013). Hepatoma polarization limits CD81 and hepatitis C virus dynamics. Cell. Microbiol. *15*, 430–445.

Hsu, M., Zhang, J., Flint, M., Logvinoff, C., Cheng-Mayer, C., Rice, C.M., and McKeating, J.A. (2003). Hepatitis C virus glycoproteins mediate pH-dependent cell entry of pseudotyped retroviral particles. Proc. Natl. Acad. Sci. USA *100*, 7271–7276.

Ibrahim, N., Wicklund, A., and Wiebe, M.S. (2011). Molecular characterization of the host defense activity of the barrier to autointegration factor against vaccinia virus. J. Virol. *85*, 11588–11600.

Keilhauer, E.C., Hein, M.Y., and Mann, M. (2015). Accurate protein complex retrieval by affinity enrichment mass spectrometry (AE-MS) rather than affinity purification mass spectrometry (AP-MS). Mol. Cell. Proteomics *14*, 120–135.

Lavanchy, D. (2011). Evolving epidemiology of hepatitis C virus. Clin. Microbiol. Infect. *17*, 107–115.

Law, G.L., Korth, M.J., Benecke, A.G., and Katze, M.G. (2013). Systems virology: host-directed approaches to viral pathogenesis and drug targeting. Nat. Rev. Microbiol. *11*, 455–466.

Lisinski, I., Matsumoto, H., Yver, D.R., Schürmann, A., Cushman, S.W., and Al-Hasani, H. (2006). Identification and characterization of p49/STRAP as a novel GLUT4-binding protein. Biochem. Biophys. Res. Commun. *344*, 1179–1185.

Lupberger, J., Zeisel, M.B., Xiao, F., Thumann, C., Fofana, I., Zona, L., Davis, C., Mee, C.J., Turek, M., Gorke, S., et al. (2011). EGFR and EphA2 are host factors for hepatitis C virus entry and possible targets for antiviral therapy. Nat. Med. *17*, 589–595.

Ma, G., Greenwell-Wild, T., Lei, K., Jin, W., Swisher, J., Hardegen, N., Wild, C.T., and Wahl, S.M. (2004). Secretory leukocyte protease inhibitor binds to annexin II, a cofactor for macrophage HIV-1 infection. J. Exp. Med. *200*, 1337–1346.

Malhotra, R., Ward, M., Bright, H., Priest, R., Foster, M.R., Hurle, M., Blair, E., and Bird, M. (2003). Isolation and characterisation of potential respiratory syncytial virus receptor(s) on epithelial cells. Microbes Infect. *5*, 123–133.

Meissner, F., and Mann, M. (2014). Quantitative shotgun proteomics: considerations for a high-quality workflow in immunology. Nat. Immunol. *15*, 112–117.

Mercer, J., Schelhaas, M., and Helenius, A. (2010). Virus entry by endocytosis. Annu. Rev. Biochem. *79*, 803–833.

Montpellier, C., Tews, B.A., Poitrimole, J., Rocha-Perugini, V., D'Arienzo, V., Potel, J., Zhang, X.A., Rubinstein, E., Dubuisson, J., and Cocquerel, L. (2011). Interacting regions of CD81 and two of its partners, EWI-2 and EWI-2wint, and their effect on hepatitis C virus infection. J. Biol. Chem. *286*, 13954–13965.

Muthumani, K., Choo, A.Y., Zong, W.X., Madesh, M., Hwang, D.S., Premkumar, A., Thieu, K.P., Emmanuel, J., Kumar, S., Thompson, C.B., and Weiner, D.B. (2006). The HIV-1 Vpr and glucocorticoid receptor complex is a gain-of-function interaction that prevents the nuclear localization of PARP-1. Nat. Cell Biol. *8*, 170–179.

Nielsen, E., Severin, F., Backer, J.M., Hyman, A.A., and Zerial, M. (1999). Rab5 regulates motility of early endosomes on microtubules. Nat. Cell Biol. *1*, 376–382.

Olson, E.N., and Nordheim, A. (2010). Linking actin dynamics and gene transcription to drive cellular motile functions. Nat. Rev. Mol. Cell Biol. *11*, 353–365.

Ong, S.E., Blagoev, B., Kratchmarova, I., Kristensen, D.B., Steen, H., Pandey, A., and Mann, M. (2002). Stable isotope labeling by amino acids in cell culture, SILAC, as a simple and accurate approach to expression proteomics. Mol. Cell. Proteomics *1*, 376–386.

Orchard, S., Ammari, M., Aranda, B., Breuza, L., Briganti, L., Broackes-Carter, F., Campbell, N.H., Chavali, G., Chen, C., del-Toro, N., et al. (2014). The MIntAct project—IntAct as a common curation platform for 11 molecular interaction databases. Nucleic Acids Res. *42*, D358–D363.

Park, E., and Griffin, D.E. (2009). Interaction of Sindbis virus non-structural protein 3 with poly(ADP-ribose) polymerase 1 in neuronal cells. J. Gen. Virol. *90*, 2073–2080.

Piccoli, C., Quarato, G., Ripoli, M., D'Aprile, A., Scrima, R., Cela, O., Boffoli, D., Moradpour, D., and Capitanio, N. (2009). HCV infection induces mitochondrial bioenergetic unbalance: causes and effects. Biochim. Biophys. Acta *1787*, 539–546.

Pileri, P., Uematsu, Y., Campagnoli, S., Galli, G., Falugi, F., Petracca, R., Weiner, A.J., Houghton, M., Rosa, D., Grandi, G., and Abrignani, S. (1998). Binding of hepatitis C virus to CD81. Science *282*, 938–941.

Ploss, A., Evans, M.J., Gaysinskaya, V.A., Panis, M., You, H., de Jong, Y.P., and Rice, C.M. (2009). Human occludin is a hepatitis C virus entry factor required for infection of mouse cells. Nature *457*, 882–886.

Rajesh, S., Sridhar, P., Tews, B.A., Fénéant, L., Cocquerel, L., Ward, D.G., Berditchevski, F., and Overduin, M. (2012). Structural basis of ligand interactions of the large extracellular domain of tetraspanin CD81. J. Virol. *86*, 9606–9616.

Raynor, C.M., Wright, J.F., Waisman, D.M., and Pryzdial, E.L. (1999). Annexin II enhances cytomegalovirus binding and fusion to phospholipid membranes. Biochemistry *38*, 5089–5095.

Reiss, S., Rebhan, I., Backes, P., Romero-Brey, I., Erfle, H., Matula, P., Kaderali, L., Poenisch, M., Blankenburg, H., Hiet, M.S., et al. (2011). Recruitment and activation of a lipid kinase by hepatitis C virus NS5A is essential for integrity of the membranous replication compartment. Cell Host Microbe *9*, 32–45.

Rieber, N., Knapp, B., Eils, R., and Kaderali, L. (2009). RNAither, an automated pipeline for the statistical analysis of high-throughput RNAi screens. Bioinformatics *25*, 678–679.

Sainz, B., Jr., Barretto, N., Martin, D.N., Hiraga, N., Imamura, M., Hussain, S., Marsh, K.A., Yu, X., Chayama, K., Alrefai, W.A., and Uprichard, S.L. (2012). Identification of the Niemann-Pick C1-like 1 cholesterol absorption receptor as a new hepatitis C virus entry factor. Nat. Med. *18*, 281–285.

Sapay, N., Guermeur, Y., and Deléage, G. (2006). Prediction of amphipathic in-plane membrane anchors in monotopic proteins using a SVM classifier. BMC Bioinformatics *7*, 255.

Scarselli, E., Ansuini, H., Cerino, R., Roccasecca, R.M., Acali, S., Filocamo, G., Traboni, C., Nicosia, A., Cortese, R., and Vitelli, A. (2002). The human scavenger receptor class B type I is a novel candidate receptor for the hepatitis C virus. EMBO J. *21*, 5017–5025.

Seeff, L.B. (2002). Natural history of chronic hepatitis C. Hepatology *36* (*1*), S35–S46.

Sharma, N.R., Mateu, G., Dreux, M., Grakoui, A., Cosset, F.L., and Melikyan, G.B. (2011). Hepatitis C virus is primed by CD81 protein for low pH-dependent fusion. J. Biol. Chem. *286*, 30361–30376.

Valiya Veettil, M., Sadagopan, S., Kerur, N., Chakraborty, S., and Chandran, B. (2010). Interaction of c-Cbl with myosin IIA regulates Bleb associated macropinocytosis of Kaposi's sarcoma-associated herpesvirus. PLoS Pathog. *6*, e1001238.

Woodham, A.W., Da Silva, D.M., Skeate, J.G., Raff, A.B., Ambroso, M.R., Brand, H.E., Isas, J.M., Langen, R., and Kast, W.M. (2012). The S100A10 subunit of the annexin A2 heterotetramer facilitates L2-mediated human papillomavirus infection. PLoS ONE *7*, e43519.

Yamauchi, Y., and Helenius, A. (2013). Virus entry at a glance. J. Cell Sci. *126*, 1289–1295.

Zhang, X., Azhar, G., Zhong, Y., and Wei, J.Y. (2004). Identification of a novel serum response factor cofactor in cardiac gene regulation. J. Biol. Chem. *279*, 55626–55632.

Zhang, X., Azhar, G., Rogers, S.C., Foster, S.R., Luo, S., and Wei, J.Y. (2014). Overexpression of p49/STRAP alters cellular cytoskeletal structure and gross anatomy in mice. BMC Cell Biol. *15*, 32.

Zona, L., Lupberger, J., Sidahmed-Adrar, N., Thumann, C., Harris, H.J., Barnes, A., Florentin, J., Tawar, R.G., Xiao, F., Turek, M., et al. (2013). HRas signal transduction promotes hepatitis C virus cell entry by triggering assembly of the host tetraspanin receptor complex. Cell Host Microbe *13*, 302–313.

Cell Reports

Supplemental Information

Quantitative Proteomics Identifies Serum Response Factor Binding Protein 1 as a Host Factor for Hepatitis C Virus Entry

Gisa Gerold, Felix Meissner, Janina Bruening, Kathrin Welsch, Paula M. Perin, Thomas F. Baumert, Florian W. Vondran, Lars Kaderali, Joseph Marcotrigiano, Abdul G. Khan, Matthias Mann, Charles M. Rice, and Thomas Pietschmann

SUPPLEMENTAL INFORMATION

SUPPLEMENTAL FIGURES AND FIGURE LEGENDS

Figure S1

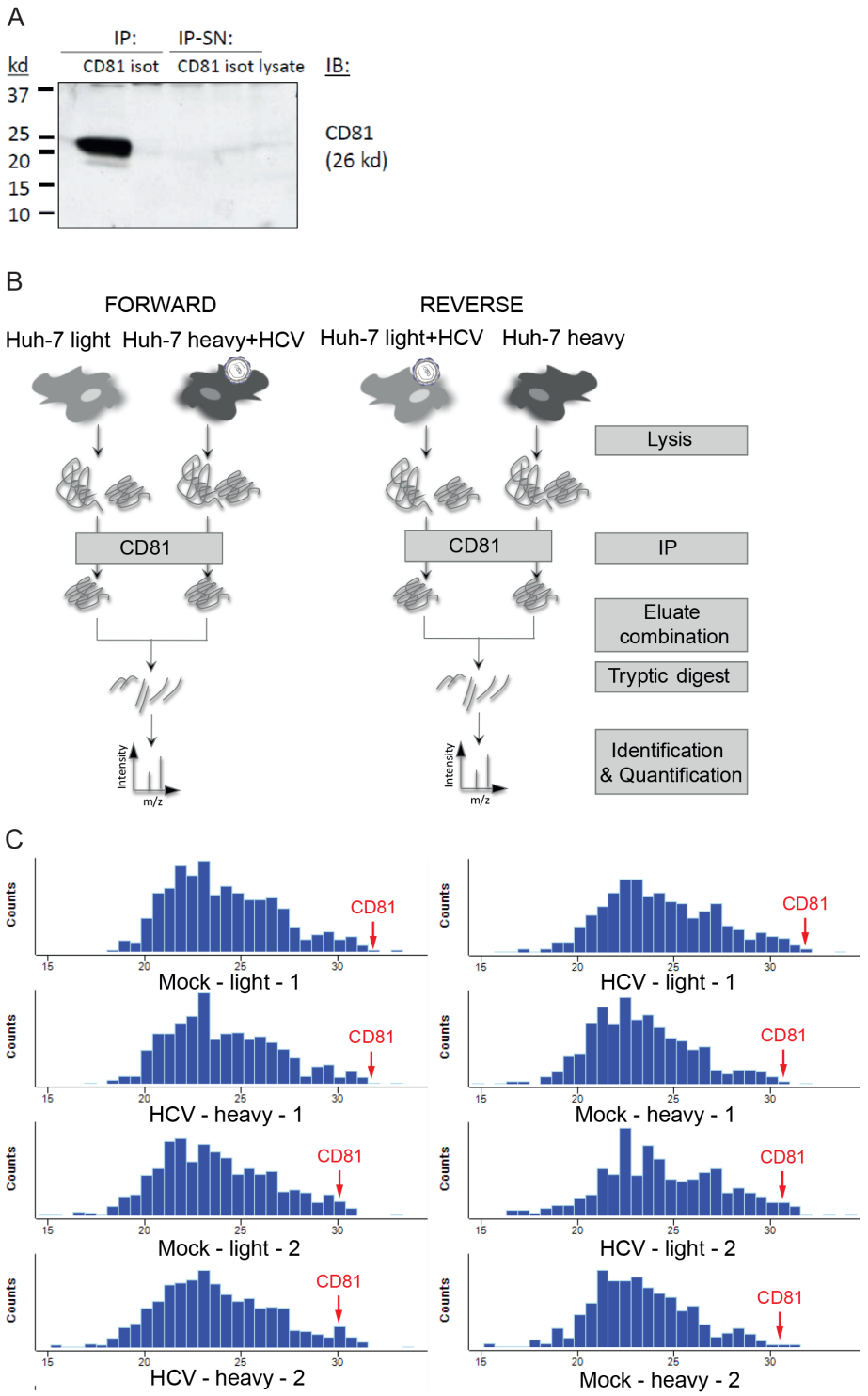

Figure S1, Related to Figure 1. Quantitative MS approach for the identification of transient HCV entry factor interactions.

(A) Immunoblot of CD81 co-IPs from resting Huh-7 cells. Cells were lysed under membrane complex preserving conditions, proteins precipitated with anti-CD81 or an isotype control antibody and lysate, IP supernatants (IP-SN) and IP eluates (IP) analyzed by immunoblot.

(B) Detailed scheme of the virus entry dependent interaction proteomics workflow. Heavy or light labeled Huh-7 cells were incubated with HCV J6/JFH clone 2 or treated with cellular supernatants from mock electroporated cells processed in the same way as the virus containing supernatants (mock). 15 min post inoculation, cells were lysed and co-immunoprecipitated with CD81 antibodies. Proteins from the two conditions were mixed, tryptically digested to peptides and analyzed by LC-MS/MS analysis. For both the forward (heavy: HCV; light: mock) and the reverse (heavy: mock; light: HCV) experiments two biological replicates were generated and analyzed.

(C) Distribution of protein abundances from heavy and light labeled IPs in four biological replicates. Ion intensities (x-axis) are plotted against counts of detected ions (y-axis). CD81 (red arrow) is reproducibly detected with highest intensities in all samples independently of the presence of HCV.

Figure S2

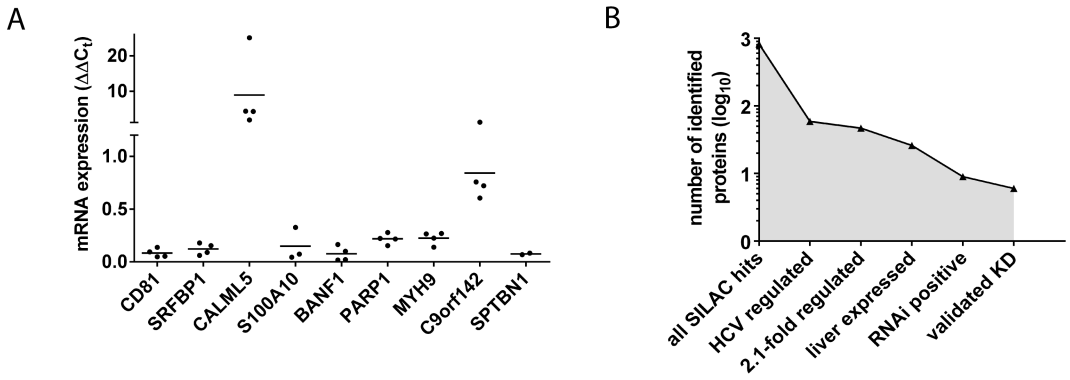

Figure S2, Related to Figure 2. Identification of CD81 associating HCV entry co-factors.

(A) RNAi validation by quantitative RT PCR. Six of the eight successful siRNA pools reduced transcript levels to 25% or less. Transcript levels of Huh-7.5 cells 48 hpt with siRNAs were measured by SYBRgreen assay and normalized to GAPDH transcripts and scrambled siRNA controls. Four biological replicates with three technical replicates each are shown.

(B) Statistics of the combined SILAC co-IP RNAi strategy. Stringent hit criteria revealed 26 HCV dependent CD81 binding partners, which are liver expressed and not exclusively localized to the nucleus. Six of these decrease HCV infectivity upon RNAi.

Figure S3

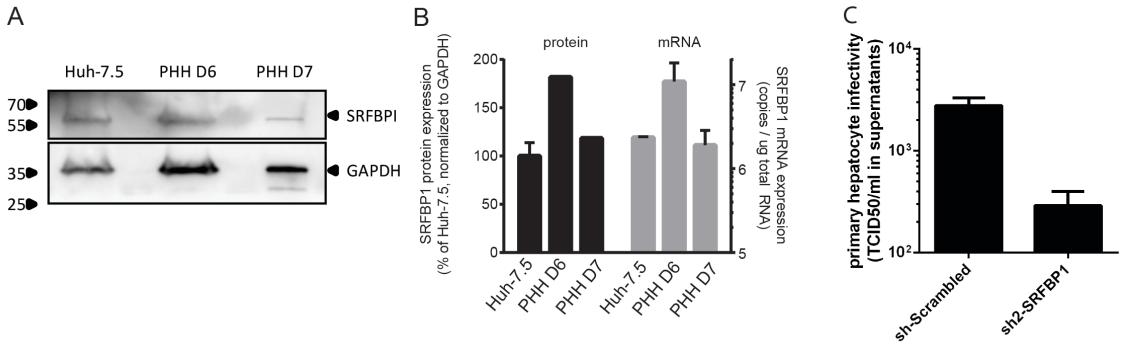

Figure S3, Related to Figure 3. SRFBP1 is expressed in primary hepatocytes and required for HCV infection but not for HCV translation or replication.

(A) Immunoblot analysis of SRFBP1 in primary human hepatocyte lysates from two independent donors (PHH D6, PHH D7). GAPDH served as loading control.

(B) Quantification of SRFBP1 protein (black bars) and *SRFBP1* transcript (grey bars) levels in primary human hepatocytes from two donors (PHH D6, PHH D7) normalized to GAPDH internal controls and to Huh-7.5 cells (black bars).

(C) Primary human hepatocytes from a single donor were transduced with SRFBP1 shRNA encoding lentiviruses or a scrambled shRNA control. 24 hpt cells were infected with HCV (Jc1), washed 4 h later and supernatant collected 24 hpi. Infectious HCV in supernatants were titered on Huh-7.5 cells. Data represent mean +/- SD of two technical replicates.

Figure S4

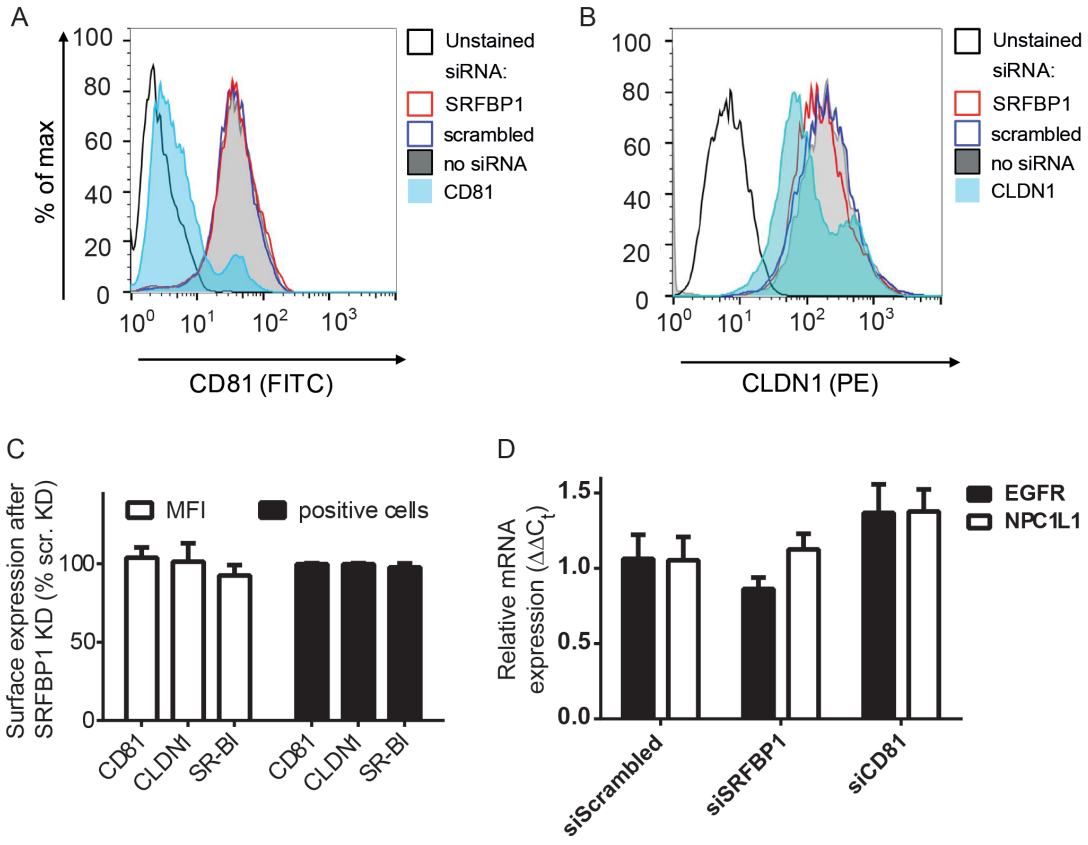

Figure S4, Related to Figure 4. Expression of HCV entry factors and co-factors in not affected by SRFBP1 silencing.

(A) Huh-7.5 cells were silenced for *SRFBP1* or *CD81* as described in Fig. 4B and surface expression levels of CD81 determined by antibody staining and flow cytometry. Unstained: FITC-conjugated isotype control antibody. The histogram is representative of four independent experiments and shows the counts of 10,000 cells per experimental condition.

(B) Flow cytometric analysis of CLDN1 as decribed in (A) after silencing for *SRFBP1* or *CLDN1.* Unstained: PE-conjugated secondary antibody only.

(C) Quantification of HCV entry factor surface expression in Huh-7.5 cells after SRFBP1 silencing analyzed by flow cytometry (see Fig. 4 B). Mean fluorescence intensity (MFI) and number of antibody positive cells were normalized to scrambled siRNA samples and expressed as mean + SD of three independent experiments.

(D) Transcript levels of the HCV entry co-factors epidermal growth factor receptor (EGFR) and Niemann-Pick C1-like protein 1 (NPC1L1) in Huh-7.5 cells 48 h post transfection with the indicated siRNAs. Expression normalized to GAPDH and siScrambled control. Mean + s.e.m. are shown.

Figure S5

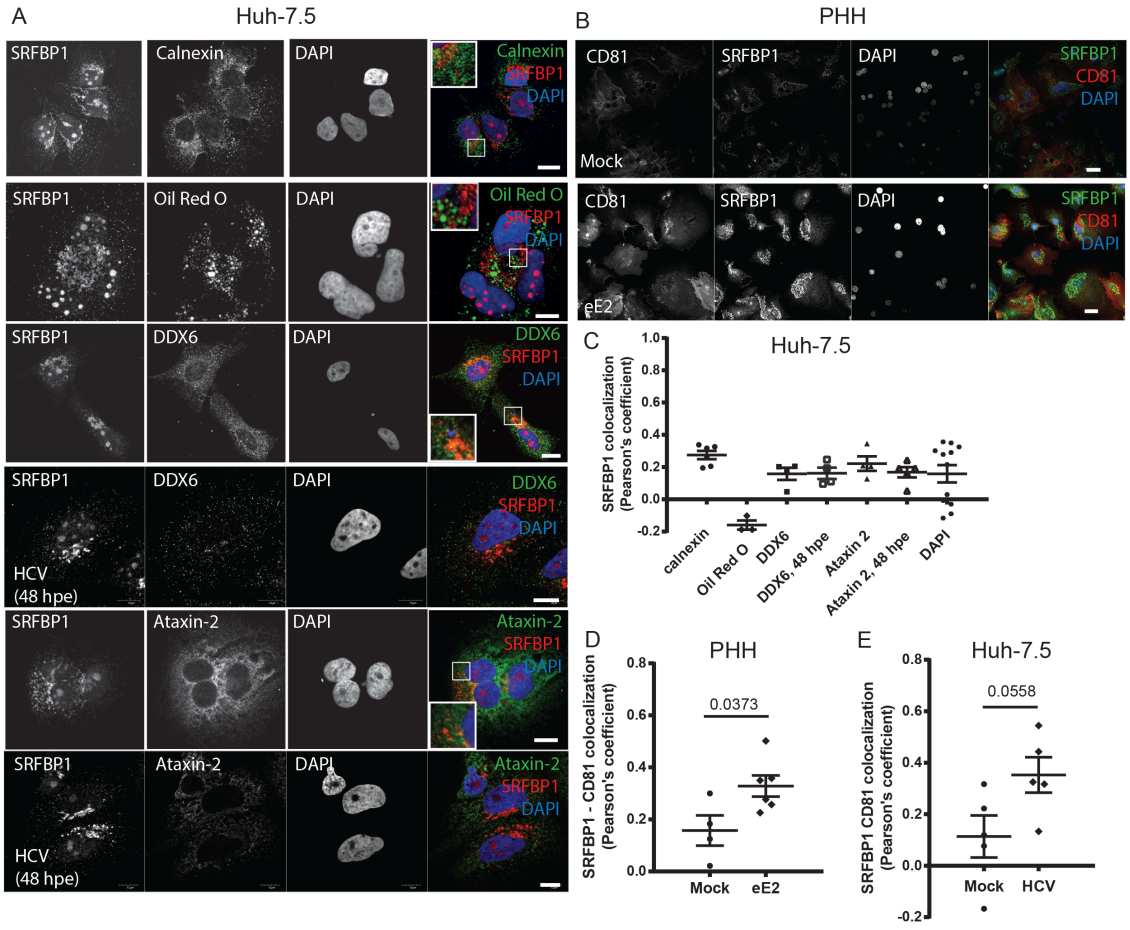

Figure S5, Related to Figure 5. SRFBP1 does not localize to the ER, lipid droplets, p bodies or stress granules in the presence and absence of HCV infection and recruits to CD81 upon eE2 exposure.

(A) Huh-7.5 cells were electroporated with HCV genotype 2a full length genomes (HCV) or left untreated and fixed 48 h later. Cells were stained for SRFBP1, the ER marker calnexin, the lipid droplet dye oil red O, the stress granule marker ataxin 2 and the p body marker DDX6 as described in Figure 4A. Insert: 2.2-fold magnification, scale bar: 10 µm.

(B) Primary human hepatocytes (PHH) were plated on collagenated cover slips, 6 h later incubated with purified eE2 or PBS (mock) for 15 min, fixed and then stained for SRFBP1 and CD81 as described in Figure 4A. Scale bar: 10 µm.

(C) Pearson's colocalization coefficient for SRFBP1 and calnexin, oil red O, DDX6, ataxin 2 or DAPI in resting Huh-7.5 cells or cells 48 h post electroporation with HCV genotype 2a full length genomes (48 hpe). Pearson's coefficients were calculated by intensity correlation analysis. Each dot represents one image frame. Mean and s.e.m. for at least four image frames are shown.

(D) Pearson's colocalization coefficient for SRFBP1 and CD81 in PHH with and without eE2 incubation for 15 min calculated by intensity correlation analysis. Each dot represents one image frame. Mean and s.e.m. for at least four image frames and p value are shown.

(E) Huh-7.5 cells were left untreated or incubated with HCV clone 2 (MOI 10) for 15 min, fixed and stained for SRFBP1 and CD81 as in Figure 4A. Pearson's colocalization coefficient for SRFBP1 and CD81 calculated by intensity correlation analysis. Each dot represents one image frame. Mean and s.e.m. for at least four image frames and p value are shown.

Figure S6

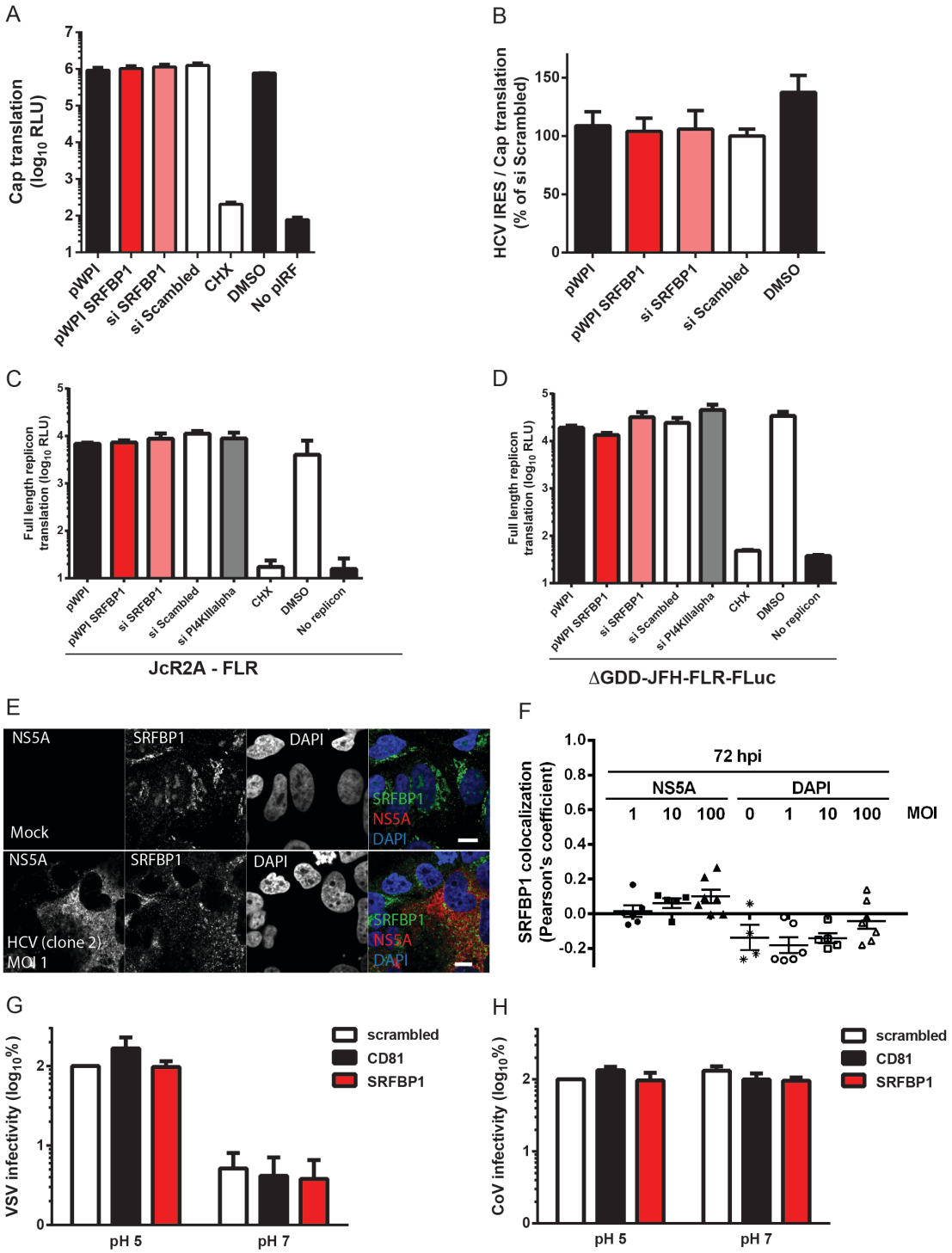
A
Cap translation (log10 RLU)
pWPI
pWPI SRFBP1
si SRFBP1
si Scambled
CHX
DMSO
No pIRF
B
HCV IRES / Cap translation (% of si Scrambled)
pWPI
pWPI SRFBP1
si SRFBP1
si Scambled
DMSO
C
Full length replicon translation (log10 RLU)
pWPI
pWPI SRFBP1
si SRFBP1
si Scambled
si PI4KIIIalpha
CHX
DMSO
No replicon
JcR2A - FLR
D
Full length replicon translation (log10 RLU)
pWPI
pWPI SRFBP1
si SRFBP1
si Scambled
si PI4KIIIalpha
CHX
DMSO
No replicon
ΔGDD-JFH-FLR-FLuc
E
NS5A
SRFBP1
DAPI
Mock
HCV (clone 2)
MOI 1
F
72 hpi
NS5A
DAPI
MOI
SRFBP1 colocalization (Pearson's coefficient)
G
VSV infectivity (log10 %)
scrambled
CD81
SRFBP1
pH 5
pH 7
H
CoV infectivity (log10 %)
scrambled
CD81
SRFBP1
pH 5
pH 7

Figure S6, Related to Figure 6. SRFBP1 is dispensable for HCV translation, replication, VSV and coronavirus infection in a plasma membrane fusion assay and does not localize to HCV replication complexes.

(A, B) Bicistronic translational reporter assay with HCV IRES driven RLuc (see Figure 6D) and cap-dependent FLuc (A). Huh-7.5 cells were transfected with the indicated siRNA or transduced with the indicated pWPI expression construct, 48 h later transfected with translational reporter RNA. 8 h after reporter transfection luciferase activity in lysates was monitored. HCV IRES dependent translation normalized to cap-dependent translation shown in (B).

(C, D) Early replication reporter assay using full length HCV genomes expressing FLuc. Huh-7.5 cells were transfected with the indicated siRNA or transduced with the indicated pWPI expression construct, 48 h later JcR2A RNA (C) or replication deficient ΔGDD-JFH-FLR-FLuc RNA (D) was transfected, cells lysed 8 hpt and luciferase activity monitored.

(E) Huh-7.5 cells were infected with HCV clone 2 (MOI 1) or left uninfected. 72 hpi cells were fixed and stained for SRFBP1 and NS5A as described in Figure 4A. Scare bar 10 μm.

(F) Pearson's colocalization coefficient for SRFBP1 and NS5A in Huh-7.5 cells 72 h post HCV clone 2 infection with the indicated MOI calculated by intensity correlation analysis. Each dot represents one image frame. Mean and s.e.m. for at least four image frames.

(G, H) Plasma membrane fusion assay was performed as depicted and described in Figure 6F. VSV*M_Q (G) or HCoV229E-luc (H) were bound to cells at 4°C in the presence of concanamycin A and plasma membrane fusion induced by washing with a buffer of the indicated pH. Infectivity was monitored 24 h later by luciferase activity quantification. Mean and s.e.m. for 4 biological replicates are shown.

Figure S7

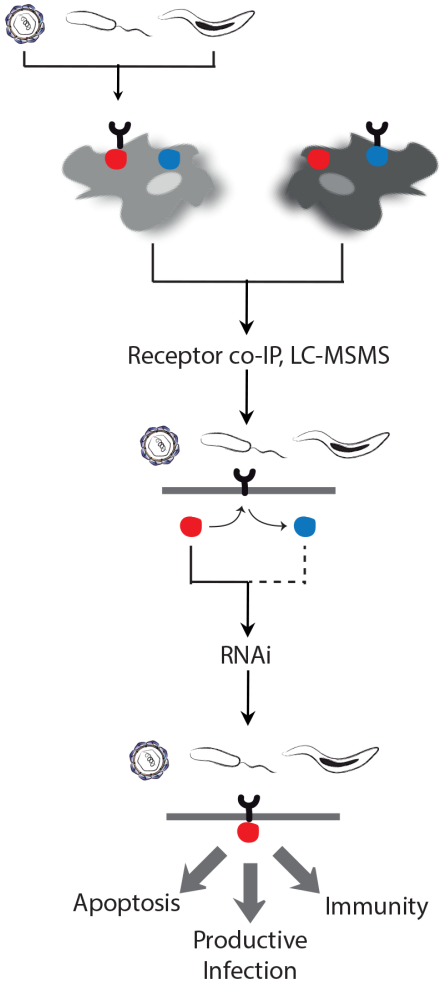

Figure S7, Related to Figure 7. Interaction proteomics workflow for the study of early host-pathogen interactions. The quantitative proteomics methodology described here is suited to reveal transient host factor - receptor interactions during pathogen entry. Briefly, susceptible cells are incubated with a pathogen or left untreated; then pathogen receptors are affinity enriched and differential receptor binding partners identified and analyzed for their functional role by RNAi. The strategy allows the identification of signaling pathways leading to cellular reprogramming like e.g. apoptosis, host factors for productive infection and innate immune sensing pathways.

SUPPLEMENTAL TABLES

Table S1, Related to Figure 1. CD81 SILAC Dataset.

SILAC ratios, heavy and light intensities for each label direction, significance analysis and protein annotations are listed. Please refer to Excel file “HCV CD81 SILAC.xlsx”.

Table S2, Related to Figure 1. HCV-dependent CD81 interactions.

Listed are the 26 selected HCV-dependent CD81 interactors, their Uniprot ID and the mean SILAC ratio of forward and reverse ratios.

Protein name	Uniprot ID	Gene name	HCV/Mock	- (Mock/ HCV)
Associating proteins				
Serum response factor-binding protein 1	Q8NEF9	*SRFBP1*	∞	n. def.
Beta-II spectrin	Q01082-3; Q01082;B2RP63;Q8WYB3	*SPTBN1*	∞	n. def.
Calpactin I light chain	P60903;Q6FGE5	*S100A10*	∞	n. def.
Huntingtin-interacting protein 12	O75146;B3KN98; B4DI31;Q6NXG8	*HIP1R*	∞	n. def.
HLA-B-associated transcript 2-like 1	Q5JSZ5-2; Q5JSZ5;Q5H9R5; Q5JSZ8;Q5JSZ5-1;Q68CR0;Q9BU62	*PRRC2B*	0,2836848	3,559736
Uncharacterized protein C9orf142	Q9BUH6-1;Q9BUH6	*C9orf142*	2,52052	3,144879
DNA-dependent protein kinase catalytic subunit	P78527-1; P78527; P78527-2; B4DL41	*PRKDC*	1,12304	2,759198
Coiled-coil domain-containing protein 124	Q96CT7	*CCDC124*	0,280723	2,387402
Barrier-to-autointegration factor	O75531;B2R4V4	*BANF1*	1,801171	1,731426
NAD(+) ADP-ribosyltransferase 1	P09874;B1ANJ4; B2R5W3;B4E0E1; Q05D33;Q96P95	*PARP1*	1,776707	1,094172
ATP-dependent DNA helicase 2 subunit 2	P13010;Q53T09; Q53TC2	*XRCC5*	1,646734	1,032336
ATP-dependent DNA helicase 2 subunit 1	P12956;B2RDN9; B1AHC8;B1AHC9; B4DE32;B4E356; Q6IC76;B1AHC7	*XRCC6*	1,584924	1,025725
Protein disulfide-isomerase A4	P13667;A8K4K6; Q549T6	*PDIA4*	1,079975	1,797987
Disscociating proteins				
Annexin A7	P20073-1	*ANXA7*	-1,351544	-0,329631
Desmoplakin	P15924-1	*DSP*	-2,391304	-2,347178
Alpha-II spectrin	Q13813-3	*SPTAN1*	0,1421349	-2,463026
Caspase-14	P31944	*CASP14*	n. def.	-2,685292
Uncharacterized protein C1orf31	Q5JTJ3-2	*C1orf31*	-2,75967	n. def.
Cellular myosin heavy chain, type A	P35579-1; P35579; A8K6E4;	*MYH9*	-0,117446	-2,799669
Protein S100-A7;Psoriasin	P31151	*S100A7*	n. def.	-3,166308
Cadherin family member 4;Desmoglein-1	Q02413	*DSG1*	-3,288417	-2,654172
Corneodesmosin;S protein	Q15517	*CDSN*	n. def.	-3,350647
Calmodulin-like protein 5	Q9NZT1	*CALML5*	n. def.	-4,130517
Collagen alpha-1(XIV) chain	Q05707-1	*COL14A1*	-4,732395	-1,932857
Cystatin-A; Cystatin-AS; Stefin-A	P01040	*CSTA*	-5,107554	-5,7702
Dermcidin	P81605;Q53YJ2; A5JHP3	*DCD*	-5,143692	n. def.

Table S3, Related to Figure 1. GOCC annotation of dynamic CD81 interactors.

Listed are the assigned GOCC categories, their accession number and the relative abundance in the dynamic CD81 interactor dataset. * Percent of hits against total number of function hits; ** Percent of hits against total number of proteins.

GO Cellular Component Category	Accession	Protein #	Relative Abundance*	Relative Abundance**
cell junction	GO:0030054	1	4.2%	7.7%
membrane	GO:0016020	2	8.3%	15.4%
cell part	GO:0044464	5	20.8%	38.5%
organelle	GO:0043226	4	16.7%	30.8%
extracellular region	GO:0005576	1	4.2%	7.7%
cell part (GO:0044464):				
plasma membrane	GO:0005886	2	40.0%	33.3%
intracellular	GO:0005622	4	80.0%	66.7%
organelle (GO:0043226):				
cytoskeleton	GO:0005856	4	100.0%	100.0%

Table S4, Related to Figure 1. GOMF annotation of dynamic CD81 interactors.

Listed are the assigned GOMF categories, their accession number and the relative abundance in the dynamic CD81 interactor dataset. * Percent of hits against total number of function hits; ** Percent of hits against total number of proteins.

GO Molecular Function Category	Accession	Protein #	Relative Abundance*	Relative Abundance**
binding	GO:0005488	14	45.2%	43.8%
catalytic activity	GO:0003824	6	19.4%	18.8%
structural molecule activity	GO:0005198	7	22.6%	21.9%
enzyme regulator activity	GO:0030234	3	9.7%	9.4%
receptor activity	GO:0004872	2	6.5%	6.3%

Table S5, Related to Figure 2. RNA interference screen scores.

Statistical analysis of the RNAi screen for CD81 interactors with a role in HCV infection. Listed are the z scores, mad and mean scores as well as SD and p values for the 26 tested targets and the CD81 and scrambled controls. MOCK: uninfected cells.

gene	score	mad	meanscore	sd	pval
scrambled 1, MOCK	-21,0668	14,7595	-21,3090	10,1301	0,0000
SRFBP1	-6,2735	6,5952	-6,3236	5,6513	0,0100
CD81	-5,7349	3,4583	-9,0317	7,0965	0,0051
CALML5	-4,2423	4,3129	-3,7624	2,7199	0,0032
S100A10	-3,9448	3,9451	-3,0981	3,1183	0,0176
BANF1	-3,2962	3,2283	-4,2092	2,6181	0,0013
CDSN	-2,9046	4,8357	-2,2253	4,6406	0,1882
PARP1	-2,7506	2,4199	-3,4268	2,7009	0,0052
MYH9	-2,4218	3,8065	-3,0481	3,7948	0,0425
XRCC5	-2,4117	2,8505	-1,8665	3,9261	0,1916
C9orf142	-2,3315	1,6008	-3,0271	2,2362	0,0036
DSG1	-1,9096	5,9350	-0,9646	5,2221	0,5946
HIP1R	-1,6771	2,5536	-1,9805	2,0093	0,0182
PRRC2B	-1,4571	1,3322	-1,1669	1,4441	0,0416
CCDC124	-1,0188	1,3338	-0,9518	1,5889	0,1101
SPTBN1	-0,8147	2,1630	-2,8339	3,4895	0,0408
PDIA4	-0,4584	2,0102	-1,1406	2,9634	0,2815
DCD	-0,1385	3,4922	-0,8216	2,7649	0,3987
ANXA7	-0,0843	1,0327	-0,1850	1,3066	0,6821
scrambled 1	0,0000	1,0000	-0,0420	1,8602	0,8931
SPTAN1	0,0044	0,7141	-0,6366	2,1065	0,3911
XRCC6	0,1374	1,3511	0,0182	2,3757	0,9822
S100A7	0,1913	1,2528	-0,5096	2,0425	0,4756
COL14A1	0,9827	1,1261	0,1357	3,2186	0,9024
C1orf31	1,5462	1,8941	1,6603	2,3879	0,0705
DSP	1,2293	1,8185	1,7334	1,8029	0,0204
CASP14	1,7643	0,8340	2,0439	1,4669	0,0031
PRKDC	2,0198	2,8057	1,7071	2,7600	0,1006
CSTA	2,0260	2,6606	1,9963	1,7432	0,0089

Table. S6, Related to Figure 2. Dynamic CD81 binding proteins with a role in HCV infection.

The six CD81 interactors with a putative role in HCV infection are listed. The average SILAC score, RNAi screen z score, silencing efficiency, endogenous protein function and previously reported role in virus infection are shown.

Gene Name	Uniprot ID	MW (kd)	Average SILAC score [log2(HCV/ mock)]	RNAi phenotype [z score]	RNAi efficiency [% of control siRNA]	Protein Function	Role in Virus Infection
SRFBP1	Q8NEF9	48,63	∞	-6,27	12,2	transcription factor, chaperone	Unknown, this study
S100A10	P60903	11,2	∞	-3,94	14,9	signaling (EGFR target), endocytosis, exocytosis	HIV-1, papillomavirus, cytomegalovirus and repiratory syncytial virus entry
BANF1	O75531	10,06	1,77	-3,3	7,64	DNA repair	retrovirus integration, vaccinia virus DNA sensing
PARP1	P09874	113,08	1,44	-2,75	21,84	poly(ADP-ribosyl)ation	sequestered to cytoplasm by HIV-1 Vpr, component of Sindbis virus replication complex
MYH9	P35579	226,53	-1,46	-2,42	22,55	cytoskeletal movement, lamellipodial retraction	Kaposi's sarcoma-associated herpesvirus macropinocytosis
SPTBN1	Q01082	274,61	∞	-0,81 (mean-score: -2,83)	7,6	cytoskeletal movement at the plasma membrane	Unknown

SUPPLEMENTAL EXPERIMENTAL PROCEDURES

Cells, Viruses and eE2

Huh-7, Huh-7.5 and 293T cells were maintained in DMEM (Invitrogen) with 10% FBS, 2 mM L-glutamine and 0.1 mM non-essential amino acids. *In vitro* transcripts of HCV full length and subgenomic genomes were prepared and transfected as described previously (Haid et al., 2010). HCV stocks were generated by electroporation of *in vitro*-transcribed RNA into Huh-7.5 cells. HCVcc particles were harvested in DMEM containing 1.5% FCS (J6/JFH clone2, (Catanese et al., 2010; Lindenbach et al., 2005)) or 10% FCS (Jc1 (Pietschmann et al., 2006), JcR2A (Reiss et al., 2011) and intergenotypic chimeras (Haid et al., 2012)) at 48 and 72 h post electroporation, filtered through a 0.45 µm pore size membrane and concentrated using 100 kDa cutoff Amicon Ultra centrifugal filters (Millipore). Experiments with HCV were carried out under biosafety level 3* containment, in compliance with institutional and federal guidelines.

E2 ectodomain (eE2) encompassing residues 384–656 from the HCV J6 genome was expressed in GnTI− HEK293T cells and purified as described in (Khan et al., 2014).

Recombinant VSV expressing enhanced green fluorescent protein designated VSV*M_Q and VSV-FLuc was kindly provided by Gert Zimmer (Hoffmann et al., 2010). VSV*M_Q carries four attenuating mutations in the M protein and expresses GFP or FLuc from an additional transcriptional unit located between G and L. 20 hpi VSV*M_Q-infected cells were quantified by flow cytometry using a FACSCalibur or Accuri instrument (BD Bioscience). Human coronavirus 229E, in

which ORF 4 is replaced by *Renilla* luciferase, (HCoV229E-luc) was kindly provided by Volker Thiel (Pfefferle et al., 2011). Infectivity was measured 24 hpi by quantification of luciferase activity in lysates. All virus titers (50% tissue culture infective dose/ml) were calculated after serial dilution based on the 50% endpoint method of Reed and Muench (Ozanne, 1984).

Lentiviral pseudoparticles with no envelope or carrying HCV or VSV glycoproteins were generated by triple transfection of 293T cells with envelope protein expression constructs pcZ.VSV.Gwt, pcDNA3.ΔcE1E2 of the HCV isolates J6 and H77 or an empty vector control, HIV-1 gag-pol expression construct pCMV.DR8.74, and *Firefly* luciferase encoding lentiviral proplasmid pWPI.FLuc. 24 h post transfection media was changed to DMEM containing 3% FCS and lentiviral pseudoparticles were harvested 48 and 72 h post transfection. Pooled supernatants were supplemented with 20 mM Hepes and 5 µg/ml polybrene and used immediately for transduction of target cells.

Primary Human Hepatocytes

Primary human hepatocytes were isolated from liver specimens obtained after partial hepatectomy and plated on collagen at a density of $1.3x10^6$ cells in P6 dishes as described in (Kleine et al., 2014). Cells were kept in hepatocyte culture medium (Lonza) and transduced with lentiviral pseudoparticles encoding an shRNA targeting SRFBP1 one day post plating. Pseudoparticles were removed 5 h post transduction and cells infected with Jc1 HCVcc 19 h later. 5 h post infection, cells were washed three times with PBS and hepatocyte culture

medium added. 24 h post infection supernatants were titrated on Huh-7.5 and cells lysed for RNA isolation to confirm SRFBP1 sliencing. HCV titers were determined by NS5A immunocytochemistry at 72 h.

Immunoprecipitation for SILAC

One-step immunoprecipitations of membrane proteins were performed by adapting the protocol of (Schneider et al., 1982) to a commercial crosslinking IP kit (Pierce). In detail, isotope labeled cells were incubated with HCV for 15 min, washed once with ice-cold PBS and scraped into ice-cold PBS before pelleting. Cells were then lysed with 1 ml/P150 IP buffer (1% NP40, 10% glycerol, 1 mM $CaCl_2$, 100 mM NaCl in 50 mM Hepes, pH 7.4) supplemented with EDTA-free protease inhibitor mix (Sigma) on ice for 30 min. Nuclear debris was pelleted at 12000xg for 10 min at 4°C. Lysates were precleared with 70ul protein blocked A/G agarose slurry/1ml lysate for 60 min at 4°C rotating, loaded onto equilibrated anti-CD81 (Santa Cruz, # sc-7637) and isotype (BD Bioscience, #555746) agarose columns (Pierce, antibodies crosslinked with disuccinimidyl suberate to protein A/G agarose according to manufacturer's instructions) and precipitated o/n at 4°C rotating. Flowthroughs were collected, beads from heavy and light conditions combined and washed three times with IP buffer. Proteins were eluted stepwise with 100 mM glycine (pH 2.8) and precipitated o/n with five volumes of ethanol and 100 mM Na-acetate (pH 5.0) using glycogen as precipitation helper. Equivalent volumes of IP lysate input, flowthrough and eluate were kept for immunoblot quality control.

LC MS/MS Analysis

Proteins were denatured, reduced, alkylated and digested with trypsin as described in (Butter et al., 2012; Meissner et al., 2013). Peptides were desalted on reversed phase C18 StageTips and acidified with 2% acetonitrile, 0.1% trifluoroacetic acid in 0.1% formic acid. A nanoflow UHPLC instrument (Thermo Fisher Scientific) was coupled on-line to an Orbitrap Elite™ Hybrid Ion Trap-Orbitrap mass spectrometer (Thermo Fisher Scientific) with a nanoelectrospray ion source (Thermo Fisher Scientific). Peptides were loaded onto a C18-reversed phase column, separated and MS data acquired using Xcalibur software. Peptides were separated by HPLC over a 150 min gradient from 2% to 60% acetonitrile and analyzed in an Orbitrap Elite mass spectrometer (Thermo Fisher Scientific). Full-scan MS was acquired with 120,000 resolution in the Orbitrap analyzer, and up to the ten-most intense ions from each full scan were fragmented with collision-induced dissociation and analyzed in the linear ion trap.

MS Bioinformatics

Mass spectra were analyzed using MaxQuant software version 1.2.6.1. Carbamidomethylcysteine was set as a fixed modification, N-terminal acetylation and methionine oxidation as variable modifications. The spectra were searched by the Andromeda search engine against the human International Protein Index protein sequence database (IPI version 3.68) combined with 248 common contaminants and concatenated with the reversed versions of all sequences. Protein identification required at least one unique or razor peptide per protein

group. The required false positive rate was set to 1% at the peptide and 1% at the protein level, and the minimum required peptide length was set to 6 amino acids. Contaminants, reverse identification and proteins only identified by site were excluded from further data analysis, which was performed in Perseus (Cox and Mann, 2012).

PANTHER and DAVID Annotation Clustering Network and Combined DAVID/STRING Functional Gene View

We performed functional annotation clustering and enrichment scoring of all 26 SILAC hits using PANTHER (Thomas et al., 2003) (Fig. 1D and 1E) or DAVID (http://david.abcc.ncifcrf.gov) version 6.7, with ‘‘high’’ classification stringency settings (Huang da et al., 2009) (Fig. 1F). DAVID analysis yielded 12 highly enriched clusters (EASE score above 1) and 17 clusters in total. We next generated a combined network view based on STRING database interactions and DAVID functional annotation clustering using a Matlab script described in (Mercer et al., 2012) and Cytoscape for visualization. Briefly, we used STRING 9.1 (http://www.string-db.org) to generate interaction networks of significant SILAC hits with a 2.1-fold or stronger dynamic CD81 interaction (Franceschini et al., 2013). Then, each protein was assigned to the cluster with the highest enrichment, in which the protein was present in the highest fraction of individual annotations. Selected unclustered proteins were placed back in the visualization as inverted arrowheads. All STRING interactions (solid lines) with a confidence score of 0.9 or higher, and all interactions of 0.35 or higher between genes within

the same functional annotation cluster were added. Finally, we manually placed functional annotation clusters in their approximate cellular locations. Selected proteins with two cellular locations were placed into both respective places (see Figure 1F).

RNAi Screen for HCV Host Factors and Bioinformatic Analysis

Huh-7.5 cells stably expressing *Firefly* luciferase (Huh-7.5 FLuc) were seeded at a density of $3x10^4$ cells per well in a 96 well plate 5 h prior to transfection (Gentzsch et al., 2011). RNA interference against the 28 dynamic CD81 interaction partners was achieved with a pool of three independent targeting siRNAs (Ambion Silencer Select). When available validated siRNA were selected. Two scrambled siRNAs served as negative and a pool of three CD81 targeting siRNAs as positive control. To avoid plate effects, four scrambled controls were randomly positioned on the plate and edges were left untreated. We transfected 0.5 pmoles of each siRNA per 96 well using lipofectamine RNAiMax (Invitrogen) according to the manufacturer's instructions. Cells were infected with the *Renilla* luciferase reporter virus JcR2A 48 h post transfection (MOI 0.1) and the inoculum replaced with medium 4 h later. Infectivity was assayed 48 hpi by quantification of *Firefly* and *Renilla* luciferase activity. Residual plate effects were computationally accounted for by normalization to the scrambled control reads. We observed no effect on cell proliferation or viability with the 28 targeting siRNA pools. The CD81 siRNA pool reduced cell proliferation in accordance with the described proliferative role of CD81 (Oren et

al., 1990). In order to eliminate proliferation dependent effects, the specific HCV infectivity was calculated by normalization of *Renilla* luciferase activity (infectivity readout) to *Firefly* luciferase activity (viability readout).

HCVcc Infection and Whole Life Cycle Assay

Huh-7.5 FLuc cells were electroporated with HCV JcR2A RNA and plated in a 24 well dish (Gentzsch et al., 2011). We transfected a pool of three siRNAs (2.5 pmol per well of each siRNA) using Lipofectamine RNAiMax five hours after electroporation according to the manufacturer's instructions (Invitrogen). 72 and 96 h post electroporation supernatants were collected and used to infect naïve cells. The latter cells were analyzed 72 hpi to evaluate a role of the targeted gene in assembly and release. At the same time producer cell lysates were collected at 72 and 96 h post electroporation to assay for a role of the target gene in HCV replication. HCV replication as well as assembly and release were quantified by assaying for *Renilla* luciferase activity in producer and receiver cell lysates. Cell viability was assessed by *Firefly* luciferase activity measurement in the same lysates. Assembly and release values were normalized for replication values to exclude that impaired replication would influence assembly and release readouts.

Pseudoparticle Infection

Huh-7.5 cells were transduced with lentiviral pseudoparticles encoding *Firefly* luciferase 48 h post siRNA silencing. Luciferase activity was determined and

HCVpp specific infectivity calculated by normalization to VSV pseudotypes and a scambled siRNA control.

Plasma Membrane Fusion Assay

To assay for endosomal acidification independent HCV uptake, we adapted a previously described membrane fusion assay (Bitzegeio et al., 2010; Tscherne et al., 2006). Briefly, Huh-7.5 cells were plated at a density of $5x10^5$ cells per 6-well in poly-lysine treated dishes and transfected with 5 nM concanamycin A to prevent acidification of endosomal compartments and thereby block the natural route of HCV entry. Concentrated virus (HCV JcR2A, HCoV229E-luc, VSV-FLuc) was allowed to bind to the cells for 2 h at 4°C in the presence of concanamycin A. After two PBS washes cells were shifted to 37°C for 1 h in the continuous presence of concanamycin A to allow glycoprotein priming. Membrane fusion was induced by a 5 min wash with pH 5 citric acid buffer. Background infection was assessed by a 5 min wash with pH 7 citric acid buffer. To complete virus uptake, cells were incubated for an additional 3 h with medium containing concanamycin A, then medium replaced and luciferase activity measured 24 hpi (HCoV229E-luc, VSV-FLuc) and 48 hpi (HCV JcR2A).

Translational Reporter Assay

The pIRF bicistronic reporter plasmid was kindly provided by Annie Cahour, Jean Dubuisson and Yves Rouille and in vitro transcribed and capped as described in (Laporte et al., 2000). Full length (pFK_i389F-Luc-EI-Core-5B/JFH1_dg) and

subgenomic (pFK_i389LucNS2-3'_JFH_dg) HCV constructs and their polymerase deficient ΔGDD mutants were transcribed as described previously (Haid et al., 2010). Huh-7.5 cells were lipofected with 1 ug RNA per 96-well and translational activity measured after 8 h by assessing luciferase activity in cell lysates.

Immunoblot and RT-PCR

For western blot analysis, equivalent volumes of cell lysates, IP flowthroughs, IP eluates or Nycodenz gradient fractions were boiled 5 min with SDS sample buffer under reducing conditions, resolved by SDS-PAGE and transferred to PVDF membranes by electroblotting. Membranes were probed for o/n at 4°C with primary antibodies (SRFBP1, Abcam ab109598; CLDN1, Invitrogen 374900; OCLN, Invitrogen 33-1500; actin, Sigma A2228; GAPDH, Sigma G9545), for 1 h at room temperature with secondary HRP or Alexa-fluorophore conjugated antibodies and analyzed using a chemiluminescence (Intas) or fluorescence detection system (Odyssey CL, Licor).

Total cellular and viral RNA was isolated using the NucleoSpin kit according to the manufacturer's instructions (Macherey-Nagel). Absolute quantification of mature SRFBP1 transcripts and viral RNA genomes was achieved by Taqman multiplex amplification (Applied Biosystems) using the following oligonucleotides and probes: SRFBP1-F 5'-CCATgCCATgAAggAATTgAAAC-3', SRFBP1-R 5'-gCTTgTACAgCAgCTTTTAgCAC-3', SRFBP1-TM 5'-FAM-TTgCTCTTTCAgTTgCAgTAgAATCTggCT-BBQ-3'; JFH-1-F 5′-TCT GCG GAA

CCG GTG AGT A-3′, JFH-1-R 5′-GGG CAT AGA GTG GGT TTA TCC A-3′, JFH-TM 5′-FAM-AAA GGA CCC AGT CTT CCC GGC AAT T-TAMRA-3′. GAPDH served as internal standard (GAPDH-F 5′-GAA GGT GAA GGT CGG AGT C-3′, GAPDH-R 5′-GAA GAT GGT GAT GGG ATT TC-3′, GAPDH-TM 5′-TET-CAA GCT TCC CGT TCT CAG CCT-TAMRA-3′).

Quantification of SILAC hit transcripts after silencing was achieved by SYBRgreen PCR using primers selected from the Harvard PrimerBank (http://pga.mgh.harvard.edu/primerbank) and GAPDH as standard for normalization.

Flow Cytometry and Immunofluorescence Microscopy

For immunofluorescence analysis Huh-7.5 cells were plated on poly-lysine coated cover slips and where indicated washed with PBS, incubated with 2ug/ml eE2, 7.5 ug/ml E2 antibody (AP33) (Owsianka et al., 2001), or HCV (J6JFH clone 2, MOI 10) for 15 min, washed with PBS and fixed with 3% paraformaldehyde for 20 min. After three PBS washes, cells were permeabilized with 0.05% TX-100 for 4 min and incubated with primary antibodies (SRFBP1, Abcam ab109598; CD81, BD 555675; CLDN1, Invitrogen 374900; OCLN, Invitrogen 33-1500; SR-BI NK-5H8-E3; LAMP1, Abcam ab25630; EEA1, BD 612006; p230, BD 611281; LBPA, MoBiTec Z-PLBPA-1-EC; Calnexin, Abcam ab31290; GLUT4, Abcam ab166704; DDX6, Abcam ab54611; Ataxin-2, BD 611378) followed by staining with secondary Alexa-fluorophore conjugated antibodies. Membranes, F actin and G actin were stained with Alexa-conjugated WGA, phalloidin and DNAse I,

respectively, (Molecular Probes) according to the manufacturer's instructions. For lipid droplet staining with oil red O (Sigma, O0625-25G) cells were rinsed with H_2O, then with 60% isopropanol and incubated with the filtered dye solution for 2 min at room temperature followed by washes with 60% isopropanol and H_2O. DAPI counterstained cells were mounted on glass slides with ProLong Gold antifade mountant (Molecular Probes, W32466) and analyzed by confocal microscopy using an inversed confocal laser-scanning microscope (Olympus Fluoview 1000), using a 60x or 100x magnification lens. The three channels (blue, green, and red) were read in a sequential acquisition mode, with an average of 3 frames for each picture (Kalman n = 3). Data analysis was performed using FluoView (Olympus) and Image J. Intensity correlation analysis was performed using the Image J colocalization analysis plugin. Pearson's colocalization coefficients were calculated for at least four individual frames with 20-40 cells.

For flow cytometry, cells were trypsinized, quenched and surface stained with primary antibodies (CLDN1, R&D MAB4618; SR-BI, NB400-104; CD81, sc-23962) in PBS containing 1% FCS for 30 min on ice. After a brief wash, secondary PE- or Alexa488-conjugated secondary antibodies were added for 30 min on ice. Cells were washed three times and analyzed on a FACSCalibur (BD Bioscience). Data analysis was performed using FlowJo.

Flotation Assays

To assess membrane association of SRFBP1 we performed membrane flotation assays according to (Ghibaudo et al., 2004). Briefly, $2.8x10^6$ Huh-7.5 cells were plated in 10 cm dishes and transduced with SRFBP1-mycDDK encoding pseudoparticles 5 h later. 60 h post transduction cells were washed once with PBS, scraped into 10 ml ice cold PBS, pelleted and resuspended in 0.5 ml ice cold hypotonic lysis buffer (10 mM Tris-HCl, pH 7.5, 2 mM $MgCl_2$) supplemented with protease inhibitors (Sigma). After 30 min incubation on ice, cells were dounce homogenized with 12 strokes and cellular debris pelleted at 1000xg for 5 min at 4 °C. Membranes were disrupted in 200 ul lysate with 1% TX-100 for 10 min on ice. TX100 treated and untreated samples were diluted with 75% Nycodenz to a final concentration of 37,5%. 0.4 ml of this suspension was overlayed with 0.8 ml 35% Nycodenz and 0.1 ml 5% Nycodenz in PBS. Equilibrium ultracentrifugation was carried out for 22 h at 4°C in a Beckmann TLA-55 rotor at 47,000 rpm, 160 µl fractions collected and analyzed by SDS PAGE and immunoblot for SRFBP1, GAPDH and CLDN1.

SUPPLEMENTAL REFERENCES

Bitzegeio, J., *et al.* (2010). Adaptation of hepatitis C virus to mouse CD81 permits infection of mouse cells in the absence of human entry factors. PLoS pathogens *6*, e1000978.

Butter, F., *et al.* (2012). Proteome-wide analysis of disease-associated SNPs that show allele-specific transcription factor binding. PLoS Genet *8*, e1002982.

Catanese, M.T., *et al.* (2010). Role of scavenger receptor class B type I in hepatitis C virus entry: kinetics and molecular determinants. Journal of virology *84*, 34-43.

Cox, J., and Mann, M. (2012). 1D and 2D annotation enrichment: a statistical method integrating quantitative proteomics with complementary high-throughput data. BMC bioinformatics *13 Suppl 16*, S12.

Franceschini, A., *et al.* (2013). STRING v9.1: protein-protein interaction networks, with increased coverage and integration. Nucleic acids research *41*, D808-815.

Gentzsch, J., *et al.* (2011). Hepatitis C virus complete life cycle screen for identification of small molecules with pro- or antiviral activity. Antiviral research *89*, 136-148.

Ghibaudo, D., *et al.* (2004). Characterization of GB virus B polyprotein processing reveals the existence of a novel 13-kDa protein with partial homology to hepatitis C virus p7 protein. The Journal of biological chemistry *279*, 24965-24975.

Haid, S., *et al.* (2012). A plant-derived flavonoid inhibits entry of all HCV genotypes into human hepatocytes. Gastroenterology *143*, 213-222 e215.

Haid, S., *et al.* (2010). Mouse-specific residues of claudin-1 limit hepatitis C virus genotype 2a infection in a human hepatocyte cell line. Journal of virology *84*, 964-975.

Hoffmann, M., *et al.* (2010). Fusion-active glycoprotein G mediates the cytotoxicity of vesicular stomatitis virus M mutants lacking host shut-off activity. The Journal of general virology *91*, 2782-2793.

Huang da, W., *et al.* (2009). Systematic and integrative analysis of large gene lists using DAVID bioinformatics resources. Nature protocols *4*, 44-57.

Khan, A.G., *et al.* (2014). Structure of the core ectodomain of the hepatitis C virus envelope glycoprotein 2. Nature *509*, 381-384.

Kleine, M., *et al.* (2014). Explanted diseased livers - a possible source of metabolic competent primary human hepatocytes. PloS one *9*, e101386.

Laporte, J., *et al.* (2000). Comparative analysis of translation efficiencies of hepatitis C virus 5' untranslated regions among intraindividual quasispecies present in chronic infection: opposite behaviors depending on cell type. Journal of virology *74*, 10827-10833.

Lindenbach, B.D., *et al.* (2005). Complete replication of hepatitis C virus in cell culture. Science *309*, 623-626.

Meissner, F., *et al.* (2013). Direct proteomic quantification of the secretome of activated immune cells. Science *340*, 475-478.

Mercer, J.*, et al.* (2012). RNAi screening reveals proteasome- and Cullin3-dependent stages in vaccinia virus infection. Cell reports *2*, 1036-1047.
Oren, R.*, et al.* (1990). TAPA-1, the target of an antiproliferative antibody, defines a new family of transmembrane proteins. Mol Cell Biol *10*, 4007-4015.
Owsianka, A.*, et al.* (2001). Functional analysis of hepatitis C virus E2 glycoproteins and virus-like particles reveals structural dissimilarities between different forms of E2. The Journal of general virology *82*, 1877-1883.
Ozanne, G. (1984). Estimation of endpoints in biological systems. Comput Biol Med *14*, 377-384.
Pfefferle, S.*, et al.* (2011). The SARS-coronavirus-host interactome: identification of cyclophilins as target for pan-coronavirus inhibitors. PLoS pathogens *7*, e1002331.
Pietschmann, T.*, et al.* (2006). Construction and characterization of infectious intragenotypic and intergenotypic hepatitis C virus chimeras. Proceedings of the National Academy of Sciences of the United States of America *103*, 7408-7413.
Schneider, C.*, et al.* (1982). A one-step purification of membrane proteins using a high efficiency immunomatrix. The Journal of biological chemistry *257*, 10766-10769.
Thomas, P.D.*, et al.* (2003). PANTHER: a library of protein families and subfamilies indexed by function. Genome research *13*, 2129-2141.
Tscherne, D.M.*, et al.* (2006). Time- and temperature-dependent activation of hepatitis C virus for low-pH-triggered entry. Journal of virology *80*, 1734-1741.